

Resonant relaxation and the warp of the stellar disc in the Galactic centre

Bence Kocsis^{1,2,3*} and Scott Tremaine^{2†}

¹ *Harvard-Smithsonian Center for Astrophysics, 60 Garden St., Cambridge, MA 02138, USA*

² *Institute for Advanced Study, Princeton, NJ 08540, USA*

³ *Einstein Fellow*

Received —

ABSTRACT

Observations of the spatial distribution and kinematics of young stars in the Galactic centre can be interpreted as showing that the stars occupy one, or possibly two, discs of radii ~ 0.05 – 0.5 pc. The most prominent (‘clockwise’) disc exhibits a strong warp: the normals to the mean orbital planes in the inner and outer third of the disc differ by $\sim 60^\circ$. Using an analytical model based on Laplace–Lagrange theory, we show that such warps arise naturally and inevitably through vector resonant relaxation between the disc and the surrounding old stellar cluster.

Key words: Galaxy: centre – Galaxy: nucleus – celestial mechanics

1 INTRODUCTION

Black holes of mass 10^6 to $10^9 M_\odot$ are found in the centres of most galaxies. These exotic objects are the engines that drive quasars and other active galactic nuclei, and may play an important role in galaxy formation through feedback to the interstellar medium. Our own Galaxy contains a central black hole of mass $\sim 4 \times 10^6 M_\odot$ associated with the radio source Sgr A*, and thus provides a unique opportunity to explore the interactions of a nuclear black hole with the surrounding gas and stars, at spatial resolution far greater than can be achieved for any other galaxy.

Among the more remarkable components of the Galactic nucleus is the population of ~ 100 massive young stars found in the central parsec ($1 \text{ pc} = 26 \text{ arcsec}$)¹. These are mostly O supergiants and Wolf-Rayet (WR) stars, with masses $\gtrsim 20 M_\odot$, formed in a burst lasting $\lesssim 2 \text{ Myr}$ approximately $6 \pm 2 \text{ Myr}$ ago (Paumard et al. 2006). Proper motions and radial velocities are available for most of these stars (Bartko et al. 2009). In the standard description, about half of the massive stars between 1 arcsec and 10 arcsec belong to a rotating system (the ‘clockwise disc’, Levin & Beloborodov 2003), which can be modelled as a warped disc with local thickness (standard deviation of the inclinations) of about 14° and mean eccentricity of 0.3–0.45 (Bartko et al. 2009). The warp is substantial: the symmetry axis of the disc varies by 60° – 70° between 1 arcsec and

10 arcsec radius. About 20% of the stars appear to be members of a second rotating system (the ‘counter-clockwise disc’), which is thicker than the clockwise disc and inclined by 115° to the clockwise disc in the same radius range. The properties and even the existence of the counter-clockwise disc are controversial (Lu et al. 2009), even though its statistical significance is 7σ according to Bartko et al. (2010). The total mass of the two discs is 5 – $10 \times 10^3 M_\odot$ (Paumard et al. 2006). Inside 1 arcsec = 0.04 pc there is a sharp cutoff in the density of WR/O stars. The surface density of the clockwise disc is

$$\Sigma \propto r^{-\delta} \quad (1)$$

with $\delta \simeq 1.4 \pm 0.2$ between 1 arcsec and 15 arcsec (Bartko et al. 2010). The disc(s) are surrounded by a spherical cluster of old stars (Buchholz et al. 2009). The cluster of old stars is much more massive than the disc(s) – $5 \times 10^5 M_\odot$ inside the outer edge of the disc at 10 arcsec – but still $\lesssim 10\%$ of the mass of the central black hole, so the disc(s) are nearly Keplerian.

The disc(s) present a number of puzzles:

- The existence of young, massive stars implies that star formation must have occurred recently in the central parsec. This is surprising, since tidal forces from the black hole suppress star formation unless the density of the protostellar cloud is orders of magnitude larger than currently observed in this region (Morris 1993; Alexander 2005).

- The presence of two distinct discs suggests that there were two separate star-formation events. But then why do the stars in the two discs appear to have the same age to within 1 Myr (Paumard et al. 2006)?

- The complexity of the dynamical models (two intersect-

* bkocsis@cfa.harvard.edu

† tremaine@ias.edu

¹ We exclude the separate population of stars (‘S-stars’) found at much smaller radii, $\lesssim 0.5 \text{ arcsec} \sim 0.02 \text{ pc}$.

ing discs, warps, etc.) needed to explain the kinematic and spatial distribution of the disc stars suggests that some other structure may provide a better description of the data. What is the nature of this structure and why is the distribution of young stars so complicated?

In this paper we shall focus on one aspect of the Galactic-centre disc(s), their substantial warp. We shall argue that the warp arises from slowly varying stochastic torques exerted on the disc by the surrounding cluster of old stars, through the process sometimes called vector resonant relaxation. Other properties of the disc(s) may also arise through resonant relaxation, a discussion that we defer to future papers.

There is an extensive literature on warps of stellar and gaseous discs in the galactic context (for general reviews see, e.g., Binney 1992; Nelson & Tremaine 1996; Binney & Tremaine 2008). In subparsec scale accretion discs, warps can arise through relativistic frame dragging (Lense–Thirring precession) around a spinning black hole (Bardeen & Petterson 1975), radiation pressure (Petterson 1977; Pringle 1996), gravitational torques due to massive tori such as the molecular torus in the Galactic centre (Nayakshin 2005; Subr et al. 2009), a binary companion such as a second black hole orbiting inside the disc (Papaloizou, Terquem, & Lin 1998; Yu & Tremaine 2003; Yu et al. 2007), or stochastic torques from a surrounding star cluster (Bregman & Alexander 2009). The self-gravity of a stellar disc can play an important role in determining the shape of the warp (Hunter & Toomre 1969; Nelson & Tremaine 1996; Ulubay-Siddiki et al. 2009). Using N -body simulations of an isolated, initially flat and thin stellar disc that resembles the Galactic-centre disc, Cuadra et al. (2008) showed that the observed warp cannot arise from interactions among the disc stars². Nayakshin & Cuadra (2005) and Hobbs & Nayakshin (2009) have suggested that the Galactic-centre disc(s) could have been formed in a high-inclination collision between two massive gas clouds. Löckmann & Baumgardt (2009) have examined the interaction of the stellar disc with a possible massive inclined second stellar disc, and showed that the discs dissolve due to the mutual torques on timescales comparable to their age.

In this paper, we examine the evolution of an initially thin, flat disc in a near-Keplerian gravitational potential, accounting for both the self-gravity of the disc and stochastic gravitational torques from a surrounding cluster of stars. We argue that the most important torques are those that arise from the mass distribution of the cluster stars after averaging over orbital phase and apsidal angle (vector resonant relaxation) and that the self-gravity of the disc suppresses the excitation of small-scale normal modes so that vector resonant relaxation warps the disc, rather than thickening it. In §2, we discuss the timescales of various processes in the Galactic centre, and establish that vector resonant relaxation with the old cluster stars is significant for the Galactic-centre disc(s), whereas most other dynamical

relaxation processes (e.g., scalar resonant relaxation, two-body relaxation, etc.) are not. In §3, we derive an analytic solution to the time evolution of an initially flat stellar disc, based on the following approximations: (i) the orbital period and the apsidal precession period are much shorter than the timescale for the warping of the disc, so we can average the motion over the orbital phase and apsidal angle; (ii) external torques on these timescales are generated exclusively by the orbit-averaged mass distribution of the cluster stars (i.e., vector resonant relaxation), (iii) the eccentricities of the disc stars are negligible; (iv) the warping angle is small (in particular, the relative inclination between any two disc stars is small compared to their fractional difference in semi-major axis); (v) the orbits of cluster stars are uncorrelated and independent of the disc (i.e., the back-reaction of the disc on the cluster is negligible); (vi) the cluster is spherical on average (i.e., the non-spherical component of the cluster mass distribution is due solely to Poisson fluctuations from individual stars). In this case, the problem reduces to Laplace–Lagrange theory, in which the secular evolution of the disc is described by a quadratic Hamiltonian, and the disc is equivalent to a system of point masses interconnected with springs and driven by the external forces from the cluster. This system is integrable as the disc can be decomposed into independent normal modes (i.e., independent harmonic oscillators). In §4, we derive the stochastic evolution of the normal mode amplitudes and consider applications to the discs in the Galactic centre. Our conclusions are discussed in §6. The statistical equilibrium of an isolated self-gravitating stellar disc is presented in the Appendix.

In future work we shall present more general numerical models that do not require the approximation that the inclinations and eccentricities are small.

2 TIME-SCALES IN THE GALACTIC CENTRE

We now ask which dynamical processes can shape the properties of the disc over its lifetime.

Two recent estimates of the distance and mass of the black hole in the Galactic centre are $R_0 = 8.0 \pm 0.6$ kpc, $M_\bullet = (4.1 \pm 0.6) \times 10^6 M_\odot$ (Ghez et al. 2008) and $R_0 = 8.3 \pm 0.4$ kpc, $M_\bullet = (4.3 \pm 0.4) \times 10^6 M_\odot$ (Gillessen et al. 2009). For simplicity we shall adopt $R_0 = 8$ kpc and $M_\bullet = 4 \times 10^6 M_\odot$. At this distance $1 \text{ pc} = 25.8 \text{ arcsec}$ and $1 \text{ arcsec} = 0.0388 \text{ pc}$.

The times and distances derived below are plotted in Figure 1, which also shows the disc age (6 ± 2 Myr) and radial extent (0.04–0.6 pc) as a hatched bar.

Gravitational radius The gravitational radius of the black hole is

$$r_\bullet = \frac{2GM_\bullet}{c^2} = 1.18 \times 10^{12} \text{ cm}, \quad (2)$$

marked in the figure by a dashed vertical line.

Orbital frequency The orbital frequency Ω of a star with semi-major axis a is given by

$$\Omega^{-1} = \left(\frac{a^3}{GM_\bullet} \right)^{1/2} = 236 \text{ yr} \left(\frac{a}{0.1 \text{ pc}} \right)^{3/2}. \quad (3)$$

² This result is consistent with the analytic arguments below that two-body and resonant relaxation among the disc stars is unimportant.

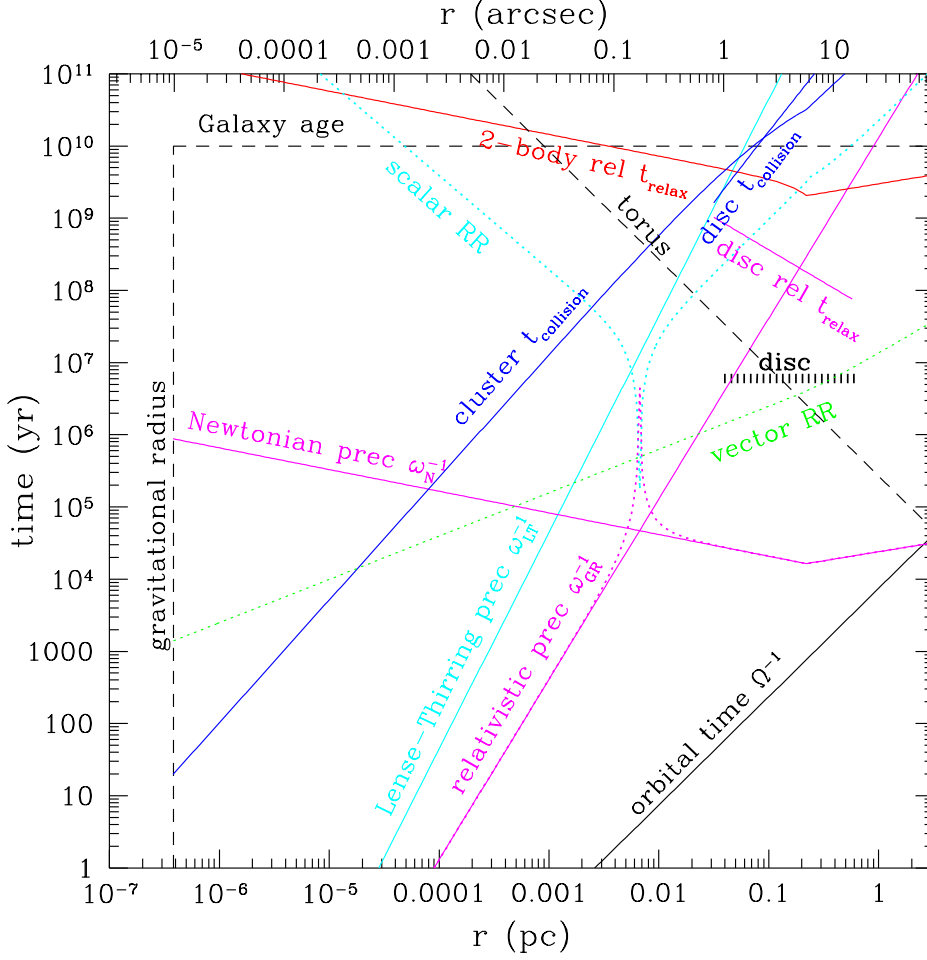


Figure 1. Time-scales in the central parsec of the Galaxy. The dashed black lines show the gravitational radius of the central black hole (eq. 2) and the age of the Galaxy. The hatched black line shows the age and radial extent of the discs(s) of WR/O stars. The slanted black line at the lower right shows the inverse orbital frequency Ω^{-1} (eq. 3). The magenta lines show the apsidal precession times due to general relativity ω_{GR}^{-1} (eq. 4) and the stellar cluster $|\omega_{\text{N}}|^{-1}$ (eq. 12), and the magenta points show the combined apsidal precession time $|\omega_{\text{GR}} + \omega_{\text{N}}|^{-1}$. The solid cyan line slanting up to the right shows the Lense–Thirring precession time (eq. 6). The red line shows the two-body relaxation time for the stellar cluster assuming that $m_2 = \langle m^2 \rangle / \langle m \rangle = 1 M_{\odot}$ (eq. 13), and a magenta line shows the two-body relaxation time within the disc, assuming $m_2 = 10 M_{\odot}$ and a disc mass of $5000 M_{\odot}$ (eq. 20). The dotted lines show the scalar and vector resonant relaxation time-scales in cyan and green, for $m_2 = 10 M_{\odot}$ (eqs. 24 and 26). The solid blue lines show the collision time in the stellar cluster for stars with mass $m = M_{\odot}$ and radius $r_{\star} = R_{\odot}$ and in the disc for $m = 20 M_{\odot}$ and radius $r_{\star} = 10 R_{\odot}$ (eqs. 21 and 23). Finally, the slanted dashed black line shows the precession time due to the molecular torus.

The characteristic orbital time Ω^{-1} (orbital period divided by 2π) is plotted in Figure 1.

Relativistic precession The apsidal precession rate due to general relativity ω_{GR} is given by

$$\omega_{\text{GR}}^{-1} = \frac{c^2 a^{5/2} (1 - e^2)}{3(GM_{\bullet})^{3/2}} = 4.11 \times 10^7 \text{ yr} (1 - e^2) \left(\frac{a}{0.1 \text{ pc}} \right)^{5/2} \quad (4)$$

where e is the eccentricity. The characteristic precession time ω_{GR}^{-1} for nearly circular orbits ($e \simeq 0$) is plotted in magenta in Figure 1. Over the radius range of the disc(s), the relativistic precession time (4) is much larger than the Newtonian precession time (12), also plotted in magenta. Thus relativistic apsidal precession is unimportant for the disc(s), although it is likely to dominate over Newtonian precession inside 0.1 arcsec.

The orbit-averaged Lense–Thirring precession of a star with angular momentum \mathbf{L} is (Landau & Lifshitz 2007)

$$\frac{d\mathbf{L}}{dt} = \frac{2G^2 M_{\bullet}^2 s}{a^3 c^3 (1 - e^2)^{3/2}} \mathbf{n}_{\bullet} \times \mathbf{L} \equiv \omega_{\text{LT}} \mathbf{n}_{\bullet} \times \mathbf{L}, \quad (5)$$

where \mathbf{n}_{\bullet} is the unit vector parallel to the spin axis of the black hole and $0 \leq s < 1$ is the spin parameter, that is, the spin angular momentum of the black hole is sGM_{\bullet}^2/c . The characteristic precession time

$$\omega_{\text{LT}}^{-1} = \frac{a^3 c^3 (1 - e^2)^{3/2}}{2G^2 M_{\bullet}^2 s} = \frac{4.45 \times 10^{10} \text{ yr}}{s} (1 - e^2)^{3/2} \left(\frac{a}{0.1 \text{ pc}} \right)^3 \quad (6)$$

is plotted in Figure 1 in cyan, for circular orbits and a maximally spinning black hole ($s = 1$). Lense–Thirring precession

is negligible for the disc(s), at least at the radii where they are currently observed ($\gtrsim 1$ arcsec).

The star cluster The black hole is surrounded by an approximately spherical cluster of old stars. The distribution of mass in the cluster can be measured from star counts by assuming that the mass density is proportional to the number density. The proportionality constant can be estimated from the kinematics (radial velocities and proper motions) of stars at radii ~ 1 pc, where the stellar mass begins to make a substantial contribution to the overall gravitational force field.

Using data from Schödel et al. (2007), Löckmann et al. (2009) estimate that the mass density at radius r is given by

$$\rho(r) = (2.8 \pm 1.3) \times 10^6 M_\odot \text{pc}^{-3} \left(\frac{r}{0.22 \text{ pc}} \right)^{-\gamma}, \quad (7)$$

with $\gamma = 1.2$ inside 0.22 pc and $\gamma = 1.75$ outside 0.22 pc. The corresponding enclosed mass is

$$\begin{aligned} \frac{M(r)}{M_\odot} &= \frac{4\pi}{M_\odot} \int_0^r \rho(x) x^2 dx \\ &= \begin{cases} 0.50 \times 10^5 (r/0.1 \text{ pc})^{1.8}, & r < 0.22 \text{ pc}, \\ 1.12 \times 10^5 (r/0.1 \text{ pc})^{1.25} - 0.92 \times 10^5, & r > 0.22 \text{ pc}, \end{cases} \end{aligned} \quad (8)$$

with an uncertainty of about 50%.

For comparison, Trippe et al. (2008) give

$$\rho(r) = 2.1 \times 10^6 M_\odot \text{pc}^{-3} \frac{1}{1 + (r/0.34 \text{ pc})^2}, \quad (9)$$

which yields an enclosed mass

$$\frac{M(r)}{M_\odot} = 1.0 \times 10^6 M_\odot f\left(\frac{r}{0.34 \text{ pc}}\right), \quad (10)$$

where $f(x) \equiv x - \tan^{-1} x$. The two expressions for $M(r)$ agree to within a factor of two for $r \gtrsim 0.3$ pc but differ by more than an order of magnitude for $r \lesssim 0.05$ pc. At $r = 1$ pc the two expressions give $M(r) = 1.9 \times 10^6 M_\odot$ and $1.7 \times 10^6 M_\odot$ respectively, somewhat larger than the independent estimate of $1.1\text{--}1.5 \times 10^6 M_\odot$ given by Schödel et al. (2009). For our numerical results we shall use the parametrization (8).

Velocity dispersion Assuming that the velocity dispersion tensor of the stellar cluster is approximately isotropic, and solving the Jeans equation for the one-dimensional velocity dispersion $\sigma(r)$ (eq. 4.216 in Binney & Tremaine 2008), we find

$$\sigma(r) = \begin{cases} 280 \text{ km s}^{-1} \sqrt{0.1 \text{ pc}/r} \sqrt{1 - 0.035 (r/0.1 \text{ pc})^{2.2}}, & \text{if } r < 0.22 \text{ pc}, \\ 250 \text{ km s}^{-1} \sqrt{0.1 \text{ pc}/r}, & \text{if } r > 0.22 \text{ pc}. \end{cases} \quad (11)$$

Newtonian precession The apsidal precession rate ω_N due to the gravitational field from a spherical star cluster is always negative, that is, the line of apsides precesses in the opposite direction to the orbital motion (e.g., Tremaine 2005). For a cluster with density $\rho(r)$ and mass $M(r) \ll M_\bullet$, the precession rate of a nearly circular orbit with radius r is

$\omega_N = -2\pi G\rho(r)/\Omega(r)$, or³

$$|\omega_N|^{-1} = \begin{cases} 2.1 \times 10^4 \text{ yr } (r/0.1 \text{ pc})^{-0.3}, & \text{if } r < 0.22 \text{ pc} \\ 1.3 \times 10^4 \text{ yr } (r/0.1 \text{ pc})^{0.25}, & \text{if } r > 0.22 \text{ pc}, \end{cases} \quad (12)$$

plotted as a magenta line in Figure 1. We also plot as magenta dots the total precession rate $\omega \equiv \omega_{\text{GR}} + \omega_N$. Over the radial extent of the disc(s), the characteristic precession time $|\omega|^{-1}$ is dominated by Newtonian effects and equal to a few times 10^4 yr, more than two orders of magnitude shorter than the disc age.

Two-body (non-resonant) relaxation The two-body relaxation time for the cluster of old stars is given by equation (7.106) in Binney & Tremaine (2008),

$$\begin{aligned} t_{\text{relax}} &= 0.34 \frac{\sigma^3}{G^2 \rho m_2 \ln \Lambda} \\ &= \begin{cases} 3.6 \times 10^9 \text{ yr } (r/0.1 \text{ pc})^{-0.3} (15/\ln \Lambda) (M_\odot/m_2) \\ \quad \times [1 - 0.035 (r/0.1 \text{ pc})^{2.2}]^{3/2}, & \text{if } r < 0.22 \text{ pc} \\ 1.7 \times 10^9 \text{ yr } (r/0.1 \text{ pc})^{0.25} (15/\ln \Lambda) (M_\odot/m_2), & \text{if } r > 0.22 \text{ pc}, \end{cases} \end{aligned} \quad (13)$$

where $\ln \Lambda \simeq \ln(M_\bullet/m) \simeq 15$, and the effective mass $m_2 \equiv \langle m^2 \rangle / \langle m \rangle$ is the ratio of the mean-square stellar mass to the mean stellar mass; we shall call this the effective mass. The relaxation time t_{relax} for $\ln \Lambda = 15$ and $m_2 = M_\odot$ is plotted in red in Figure 1.

Unfortunately the effective mass is quite uncertain. We assume a stellar mass function of the form

$$dn \propto m^{-\alpha} dm \quad \text{for } m_{\text{min}} < m < m_{\text{max}}; \quad (14)$$

then if $m_{\text{min}} \ll m_{\text{max}}$,

$$m_2 = \begin{cases} (\alpha - 2)(\alpha - 3)^{-1} m_{\text{min}} & \alpha > 3; \\ (\alpha - 2)(3 - \alpha)^{-1} m_{\text{max}}^{3-\alpha} m_{\text{min}}^{\alpha-2} & 2 < \alpha < 3; \\ (2 - \alpha)(3 - \alpha)^{-1} m_{\text{max}} & \alpha < 2. \end{cases} \quad (15)$$

Thus for a standard Salpeter mass function ($\alpha = 2.35$) with $m_{\text{max}} = 100 M_\odot$ and $m_{\text{min}} = 0.1 M_\odot$, $m_2 = 4.8 M_\odot$. For the Kroupa et al. (1993) solar neighborhood mass function, $m_2 = 0.66 M_\odot$. However, there is evidence that the mass function in the Galactic centre is much more top-heavy than in the solar neighborhood. Bartko et al. (2010) suggest that the Galactic-centre disc(s) have $\alpha \simeq 0.45$, in which case $m_2 = 0.6 m_{\text{max}} \sim 60 M_\odot$. Even if the initial mass function were known, there are other complications. First, the initial-final mass function – the relation between the main-sequence stellar mass and the mass of the compact object that remains after stellar evolution is complete – is poorly known. Second, star clusters, massive gas clouds, and other density inhomogeneities also contribute to m_2 and may lead to values of m_2 that are orders of magnitude larger than the typical stellar mass (Perets et al. 2007). An example in the Galactic Centre is IRS 13E, a compact cluster of three bright blue supergiants and many fainter components with a

³ This formula was derived for eccentricity $e \ll 1$, but works fairly well for $e \lesssim 1$. For example, if the cluster density is a power law in radius, $\rho(r) \propto r^{-\gamma}$ with $1 < \gamma < 3$, the error is less than 30% for all eccentricities $e < 0.7$.

velocity dispersion suggesting a central mass of a few $10^4 M_\odot$ (Fritz et al. 2010).

A further uncertainty is that two-body relaxation may lead to mass segregation so that the effective mass depends on radius. In particular, the relaxation time inside a few tenths of a parsec may be dominated by stellar remnants rather than stars (O’Leary et al. 2009). If the mass function is broad and dominated by light stars, then the heavy stars develop a much steeper cusp with $\rho \propto r^{-2}$ to r^{-3} . This affects m_2 primarily very close to the black hole, increasing m_2 by a factor of ~ 2 at 0.4 pc and a factor ~ 4 at 0.04 pc (Alexander & Hopman 2009; Keshet et al. 2009).

The two-body relaxation time for $m_2 = 1 M_\odot$ shown in Figure 1 is never shorter than a few Gyr so even if $m_2 \sim 10^2 M_\odot$ two-body relaxation is negligible over the age of the disc stars, $\lesssim 10$ Myr. However, two-body relaxation may have a substantial effect on old stars in the surrounding cluster.

For massive stars such as the WR/O stars observed in the disc(s), dynamical friction from the star cluster can act on a shorter time-scale than t_{relax} . The time-scale for orbital decay of a star of mass m on a near-Keplerian circular orbit of radius r is given by

$$t_{\text{fric}}^{-1} \equiv \frac{1}{r} \frac{dr}{dt} = 8\pi\Omega \frac{m}{M_\bullet} \frac{\rho r^3}{M_\bullet} \ln \Lambda g(X), \quad (16)$$

where $g(X) = \text{erf}(X) - X \text{erf}'(X)$ and $X = v/(\sqrt{2}\sigma)$ where v is the circular speed at r (Binney & Tremaine 2008)⁴. If the density varies as a power law with radius, $\rho \propto r^{-\gamma}$, then $X = [\frac{1}{2}(1+\gamma)]^{1/2}$. Using $v = (GM_\bullet/r)^{1/2}$ and the dispersion profile (11), we find that $g(X)$ varies from 0.47 for $r \ll 0.2$ pc to 0.57 for $r \gg 0.2$ pc so for our purposes it is adequate to use a constant value $g(X) = 0.5$. With this approximation

$$t_{\text{fric}} = \begin{cases} 1.7 \times 10^8 \text{ yr } (r/0.1 \text{ pc})^{-0.3} (12/\ln \Lambda)(20 M_\odot/m), & \text{if } r < 0.22 \text{ pc}, \\ 1.1 \times 10^8 \text{ yr } (r/0.1 \text{ pc})^{0.25} (12/\ln \Lambda)(20 M_\odot/m), & \text{if } r > 0.22 \text{ pc}. \end{cases} \quad (17)$$

We conclude that the action of dynamical friction from the star cluster on the disc stars is negligible over the disc age of 6 Myr, even for stars as massive as $100 M_\odot$.

The effects of two-body relaxation between the disc stars are uncertain because the properties of the disc(s) are poorly determined and the relaxation time is a strong function of the root mean squared (rms) eccentricity and inclination. For our purposes it is sufficient to approximate the disc as a single population of stars of mass m , and in this case the eccentricity relaxation time is given by (Stewart & Ida 2000)

$$t_{\text{relax}}^{-1} \equiv \frac{1}{\langle e^2 \rangle} \frac{d\langle e^2 \rangle}{dt} = 4.5 \frac{\Omega}{\langle e^2 \rangle^2} \frac{m}{M_\bullet} \frac{\Sigma r^2}{M_\bullet} \ln \Lambda. \quad (18)$$

Here $\langle e^2 \rangle$ is the mean-square eccentricity of the disc stars, $\Sigma(r)$ is the surface density, and $\Lambda \simeq \langle e^2 \rangle^{3/2} M_\bullet/m$. This formula assumes that the rms inclination $\langle i^2 \rangle^{1/2} \simeq 0.5 \langle e^2 \rangle^{1/2}$, a typical value seen in relaxed discs and consistent with observations of the clockwise disc; and that $\Lambda \gg 1$ (the disc is

‘dispersion-dominated’). The inclination relaxes at a rate

$$\frac{1}{\langle i^2 \rangle} \frac{d\langle i^2 \rangle}{dt} = \frac{0.5}{t_{\text{relax}}}. \quad (19)$$

We assume that the surface-density distribution in the disc is given by equation (1) and parametrize the disc by its total mass M_{disc} , which is probably about $5000 M_\odot$ (Paumard et al. 2006). Then

$$t_{\text{relax}} = 4 \times 10^8 \text{ yr} \frac{\langle e^2 \rangle^2}{(0.3)^4} \frac{5000 M_\odot}{M_{\text{disc}}} \frac{10 M_\odot}{m_2} \left(\frac{0.1 \text{ pc}}{r} \right)^{0.9} \frac{9}{\ln \Lambda}, \quad (20)$$

where $\ln \Lambda = 9.3$ corresponds to $m = 10 M_\odot$, $\langle e^2 \rangle^{1/2} = 0.3$. Given these parameters, the disc relaxation time is plotted in magenta in Figure 1. Even for a large effective mass, $m_2 \sim 10^2 M_\odot$, the minimum relaxation time over the radial range of the disc(s) is $\gtrsim 3 \times 10^7$ yr, so two-body relaxation should be negligible for most stars over the disc age of 6 Myr. However, if the eccentricities and inclinations in the disc have been over-estimated, perhaps because of unrecognized systematic errors, the scaling $t_{\text{relax}} \sim e^4$ implies that the relaxation time could be much shorter.

Physical collisions For a population of stars of a single mass, the rate of physical collisions is (Binney & Tremaine 2008, eq. 7.195)

$$t_{\text{coll}}^{-1} = 16\sqrt{\pi} n \sigma r_\star^2 (1 + \Theta) \quad (21)$$

where $n = \rho/m$ is the number density of stars and $\Theta \equiv \frac{1}{4} v_\star^2 / \sigma^2$ where $v_\star = \sqrt{2Gm/r_\star}$ is the escape speed from the surface of the star, radius r_\star . The collision time of stars in the cluster is shown in blue in Figure 1, assuming that the cluster is mainly composed of solar-type stars with $m = M_\odot$ and $v_\star = 618 \text{ km s}^{-1}$. At radii $\lesssim 0.01$ pc, where the collision time is less than a few Gyr, collisions are likely to play a dominant role in determining the distribution of old solar-type stars and the giants into which they eventually evolve, which have much shorter lifetimes but much larger radii. Collisional destruction of red-giant envelopes may be responsible for the depletion in luminous red giants observed inside ~ 1 pc and the disappearance of the CO spectral feature associated with red giants in the integrated light (Alexander 2005; Dale et al. 2009). However, collisions with stars in the old cluster do not play a major role in the evolution of the early-type stars in the disc(s), since the collision time is much longer than the disc age, even after accounting for the larger radii and masses of the WR/O stars.

In a dispersion-dominated disc composed of identical stars of mass m and radius r_\star , the collision rate is (e.g., Heng & Tremaine 2009)

$$t_{\text{coll}}^{-1} = 16 \frac{\Sigma}{m} \Omega r_\star^2 (0.69 + 1.52\Theta), \quad \Theta = \frac{m}{M_\bullet} \frac{r}{r_\star} \frac{1}{\langle e^2 \rangle}. \quad (22)$$

With the same parameters used to derive equation (20), we find

$$t_{\text{coll}} = \frac{4.1 \times 10^{11} \text{ yr}}{1 + 2.20\Theta} \frac{5000 M_\odot}{M_{\text{disc}}} \frac{m}{20 M_\odot} \left(\frac{r}{0.1 \text{ pc}} \right)^{2.9} \left(\frac{10 R_\odot}{r_\star} \right)^2$$

$$\Theta = 24.6 \frac{m}{20 M_\odot} \frac{10 R_\odot}{r_\star} \frac{r}{0.1 \text{ pc}} \frac{(0.3)^2}{\langle e^2 \rangle}. \quad (23)$$

This result is shown as a blue line in Figure 1. The collision time is longer than the disc age.

⁴ This result assumes that the distribution function is Maxwellian but should be approximately valid for more realistic distribution functions.

Scalar resonant relaxation Resonant relaxation (Rauch & Tremaine 1996) arises from the forces due to the orbit-averaged mass distribution of the stars. Because these forces vary only slowly, they affect the angular momentum but not the energy of stellar orbits. Scalar resonant relaxation affects the magnitude of the angular momentum and thus the eccentricity, while vector resonant relaxation affects the direction of the angular momentum vector but not its magnitude. The scalar resonant relaxation time in a spherical stellar system is (Hopman & Alexander 2006)

$$t_{\text{rr},s} = \frac{4\pi|\omega|}{\beta_s^2\Omega^2} \frac{M_\bullet^2}{M(r)m_2}; \quad (24)$$

here ω is the apsidal precession rate, the sum of the (negative) Newtonian rate ω_N (eq. 12) and the (positive) relativistic rate ω_{GR} (eq. 4). The dimensionless coefficient β_s is estimated to be 1.05 ± 0.02 by Eilon et al. (2009). Using these parameters and effective mass $m_2 = 10 M_\odot$ we plot the scalar resonant relaxation time using cyan dots in Figure 1. The cuspy minimum near $r = 0.007$ pc arises where relativistic precession cancels Newtonian precession so the total precession rate vanishes⁵.

The scalar resonant relaxation time is less than 10^{10} yr throughout the central parsec. Thus the eccentricity distribution of old stars in this region should be relaxed. However, the scalar resonant relaxation time exceeds 10^8 yr throughout the radial extent of the disc(s), so eccentricity relaxation of the disc stars is likely to be small. However, it is likely that the eccentricity relaxes faster for the most massive stars in the cluster, similar to how dynamical friction (16) is faster than two-body relaxation for massive stars (Rauch & Tremaine 1996). Assuming that the analogous resonant dynamical friction time-scale is inversely proportional to stellar mass⁶, it is still comparable to the disc age only near its inner edge.

Scalar resonant relaxation can also occur among the stars in the disc(s). The rate for this process is more difficult to determine (Tremaine 1998).

Vector resonant relaxation This process affects the orientation of the angular-momentum vector but not its magnitude. In a stellar system in which the time-averaged gravitational field is spherically symmetric, the vector resonant relaxation time is (Eilon et al. 2009)⁷

$$t_{\text{rr},v} = \frac{2\pi}{\beta_v^2\Omega} M_\bullet \frac{1}{\sqrt{M(r)m_2}}. \quad (25)$$

⁵ The sharpness of this minimum is artificial, since the total precession rate vanishes at different semi-major axes for orbits of different eccentricities (Gürkan & Hopman 2007).

⁶ The rate of resonant dynamical friction can be computed using the formalism for ordinary dynamical friction derived by Tremaine & Weinberg (1984), in which the friction arises from stars that are in near-resonance with an orbiting massive body; resonant friction is stronger than ordinary friction because some of the resonant denominators are near zero.

⁷ We have set Eilon et al.'s parameter A_ϕ to unity.

Adopting $\beta_v = 1.83 \pm 0.03$ from Eilon et al. (2009), we have

$$t_{\text{rr},v} = \begin{cases} 7.9 \times 10^6 \text{ yr} \sqrt{M_\odot/m_2} (r/0.1 \text{ pc})^{0.6}, & \text{if } r < 0.22 \text{ pc}, \\ 5.3 \times 10^6 \text{ yr} \sqrt{M_\odot/m_2} (r/0.1 \text{ pc})^{0.9} \\ \quad \times [1 - 0.82(r/0.1 \text{ pc})^{-1.25}]^{-1/2}, & \text{if } r > 0.22 \text{ pc}. \end{cases} \quad (26)$$

This result is plotted in green in Figure 1, for $m_2 = 10 M_\odot$. At all radii, vector resonant relaxation is substantially faster than scalar resonant relaxation. The inclination distribution of old stars should be relaxed throughout the stellar cluster.

Equation (26) is only valid if the nodal precession rate is dominated by the stochastic component of the non-spherical gravitational force. Hence this equation may overestimate the relaxation rate if the stellar system is not spherically symmetric. For example, the non-spherical field from the disc is smaller than the stochastic field from the cluster stars only if $M_{\text{disc}} \lesssim [M(r)m_2]^{1/2}$. For $M(r) \sim 1 \times 10^5 M_\odot$ (cf. eq. 8) and $m_2 \sim 100 M_\odot$ (see discussion following eq. 15), this requires $M_{\text{disc}} \lesssim 3 \times 10^3 M_\odot$, compared to an estimated mass of $5 \times 10^3 M_\odot$. Thus the approximation that the precession rate is dominated by stochastic forces is suspect, and should be improved in future models.

Vector resonant relaxation may be responsible for warps in gaseous accretion discs in the centres of galaxies, in particular for the warp of the maser disc in the galaxy NGC 4258 (Bregman & Alexander 2009). It may also be the principal mechanism that isotropizes the inclinations of S-stars in the Galactic centre (Hopman & Alexander 2006; Perets et al. 2009). In this paper, we investigate whether vector resonant relaxation leads to the warped structure of the stellar disc in the Galactic centre (Bartko et al. 2009).

Vector resonant relaxation can also occur among the stars in the disc. Nodal precession within the disc is determined by the mean gravitational field of the flattened mass distribution, rather than the random torques from individual stars. The typical nodal precession rate for a star in the disc is⁸

$$\nu \simeq \frac{\Omega}{\langle i^2 \rangle^{1/2}} \frac{M_{\text{disc}}}{M_\bullet}. \quad (27)$$

We then estimate the vector resonant relaxation time from equation (24) by replacing the apsidal precession rate ω with the nodal precession rate ν and the cluster mass $M(r)$ with the disc mass M_{disc} :

$$t_{\text{rr},v} \simeq \frac{4\pi}{\Omega \langle i^2 \rangle^{1/2}} \frac{M_\bullet}{m_2} \\ \simeq 2.4 \times 10^9 \text{ yr} \frac{14^\circ}{\langle i^2 \rangle^{1/2}} \frac{20 M_\odot}{m_2} \left(\frac{r}{0.1 \text{ pc}} \right)^{3/2}. \quad (28)$$

This is much longer than both the age of the disc(s) and the vector resonant relaxation time-scale due to the cluster stars. Thus vector resonant relaxation among the disc stars is unlikely to play an important role in determining the properties of the Galactic-centre disc(s)⁹.

⁸ Note that the rate diverges as the thickness of the disc approaches zero, because the torque exerted on a ring by a massive, razor-thin disc approaches infinity near the disc.

⁹ Nevertheless, it is worthwhile to understand the effects of vector resonant relaxation on an old, isolated disc, and this is the subject of the Appendix.

Warping by a massive perturber The disc(s) can be warped by a massive perturber, such as the molecular torus outside the disc at 1.5–7 pc (Christopher et al. 2005) or an intermediate-mass black hole inside the disc (Yu et al. 2007). This process was first investigated by Laplace in the context of planetary satellites and has been studied by many authors since then (Hunter & Toomre 1969; Nelson & Tremaine 1996; Ulubay-Siddiki et al. 2009); see Nayakshin (2005), Löckmann & Baumgardt (2009), and Subr et al. (2009) in the context of the Galactic-centre disc(s). The precession rate of a circular ring at radius r due to a circular ring of mass m_p at radius r_p with relative inclination I is given by equation (73); in the limit where $r \ll r_p$ or $r \gg r_p$ the result simplifies to (Nayakshin 2005)

$$\nu_p \simeq -\frac{3}{4}\Omega \frac{m_p}{M_\bullet} \frac{r r_{<}^2}{r_p^3} \cos I, \quad (29)$$

where $r_{<} = \min(r, r_p)$, $r_{>} = \max(r, r_p)$. This formula assumes that the mass of the perturbed ring is sufficiently small that its angular momentum is much less than the angular momentum of the perturber.

The characteristic precession time $t_p = 1/\nu_p$ for an external perturber ($r \ll r_p$) is then

$$t_p \simeq 8.5 \times 10^6 \text{ yr} \frac{10^6 M_\odot}{M_p} \left(\frac{r_p}{1.5 \text{ pc}}\right)^3 \left(\frac{0.1 \text{ pc}}{r}\right)^{3/2} \frac{0.5}{\cos I}. \quad (30)$$

The reference masses and radii have been set to resemble the molecular torus (Christopher et al. 2005). For these parameters, the precession time-scale is longer than the age of the disc at $r \lesssim 0.1$ pc. However, for $r \gtrsim 0.1$ pc, the molecular torus can warp the Galactic-centre disc(s) significantly, at least if $\cos I$ is not too small (Fig. 1). Curiously, the molecular torus is nearly orthogonal to the mean orientation of the clockwise stellar disc ($\cos I \simeq 0.00 \pm 0.03$). More precisely it is nearly orthogonal to the inner parts ($\cos I \simeq 0.05 \pm 0.03$ for $r \lesssim 0.15$ pc), but not the outer parts ($\cos I \simeq 0.52$ and 0.24 between $r = 0.13$ – 0.27 pc and 0.27 – 0.46 pc, respectively). Subr et al. (2009) argued that the molecular torus could lead to the thickening and warping of the stellar disc if it were initially not orthogonal.

The precession time for an internal perturber ($r \gg r_p$) is

$$t_p \simeq 5.7 \times 10^6 \text{ yr} \frac{5000 M_\odot}{M_p} \left(\frac{0.1 \text{ pc}}{r_p}\right)^2 \left(\frac{r}{0.2 \text{ pc}}\right)^{7/2} \frac{0.5}{\cos I}. \quad (31)$$

The reference masses and radii have been set to resemble the counter-clockwise disc (Bartko et al. 2009). For these parameters the precession time-scale is comparable to the age of the disc; in fact, Nayakshin et al. (2006) have used N -body simulations to set an upper limit of $5 \times 10^3 M_\odot$ on the mass of the counter-clockwise disc from the requirement that it does not warp the clockwise disc too much.

We have seen that a rich set of internal and external dynamical processes can affect the evolution and current state of the Galactic centre disc(s). A useful first approximation is to neglect external tidal fields, two-body relaxation, dynamical friction, scalar resonant relaxation, and scalar resonant friction with the surrounding old stellar cluster, as well as two-body and resonant relaxation between the disc stars. We shall also assume that there is no massive perturber in the

disc. We may then focus on the effects of vector resonant relaxation with the surrounding cluster. In the next sections we develop analytic machinery to provide a description of this interaction.

3 LAPLACE–LAGRANGE THEORY FOR AN ISOLATED DISC

Vector resonant relaxation affects the orientation of stellar orbits but not their semi-major axes or eccentricities. Since the relaxation time is much larger than the apsidal precession time (12) each orbit may be thought of as an axisymmetric planar annulus obtained from the Keplerian orbit by averaging over mean anomaly and argument of pericentre.

We investigate the dynamics of the disc using a simple model system. To construct this we shall assume that the stellar orbits in the disc are nearly coplanar ($I \ll 1$) and nearly circular ($e \ll 1$). In fact we shall make an even stronger assumption: that $e, I \ll \Delta a/a$ where Δa is the typical difference in semi-major axis between a star and its nearest neighbor. This condition is satisfied in many planetary systems, including our own, but probably not in the Galactic-centre disc(s); nevertheless we shall argue below that it allows an analytic treatment of resonant relaxation that captures its most important features.

With these approximations, we evaluate the Hamiltonian of a system of N stars of masses, semi-major axes, inclinations, and nodes m_i , a_i , I_i , and Ω_i , $i = 0, \dots, N-1$, to quadratic order in the eccentricity and inclination. This is the classical Laplace–Lagrange secular theory (Murray & Dermott 1999). In this theory the inclination and node are decoupled from the eccentricity and apse. The evolution of the latter two elements is scalar resonant relaxation, which we have argued is unimportant because of the relatively rapid apsidal precession induced by the stellar cusp. The evolution of the former is vector resonant relaxation; the relevant Hamiltonian is

$$H(\mathbf{q}, \mathbf{p}) = \frac{G}{8} \sum_{i=0}^{N-1} \sum_{j=i+1}^{N-1} \frac{m_i m_j}{\max(a_i, a_j)} \alpha_{ij} b_{3/2}^{(1)}(\alpha_{ij}) \times \left[\left(\frac{p_i}{\gamma_i} - \frac{p_j}{\gamma_j} \right)^2 + \left(\frac{q_i}{\gamma_i} - \frac{q_j}{\gamma_j} \right)^2 \right], \quad (32)$$

where $\alpha_{ij} = \min(a_i, a_j) / \max(a_i, a_j)$,

$$b_{3/2}^{(1)}(\alpha) = \frac{2}{\pi} \int_0^\pi \frac{\cos \theta d\theta}{(1 - 2\alpha \cos \theta + \alpha^2)^{3/2}} \quad (33)$$

is the Laplace coefficient¹⁰, $\gamma_i = m_i^{1/2} (GM_\bullet a_i)^{1/4}$, and

$$q_i \equiv \gamma_i I_i \sin \Omega_i, \quad p_i \equiv -\gamma_i I_i \cos \Omega_i \quad (36)$$

¹⁰ In terms of the complete elliptic integrals of the first and second kind

$$K(k) = \int_0^\pi \frac{d\theta}{\sqrt{1 - k^2 \sin^2 \theta}}, \quad E(k) = \int_0^\pi \sqrt{1 - k^2 \sin^2 \theta} d\theta, \quad (34)$$

the Laplace coefficient satisfies

$$b_{3/2}^{(1)}(\alpha) = \frac{4}{\pi \alpha (1 - \alpha^2)^2} [(1 + \alpha^2)E(\alpha) - (1 - \alpha^2)K(\alpha)]. \quad (35)$$

are canonical coordinates and momenta. For some purposes it is useful to ‘soften’ the Laplace coefficient to suppress the singularity at $\alpha = 1$, replacing the formula above by

$$b_{3/2}^{(1)}(\alpha, \epsilon) = \frac{2}{\pi} \int_0^\pi \frac{\cos \theta \, d\theta}{(1 - 2\alpha \cos \theta + \alpha^2 + \epsilon^2)^{3/2}} \quad (37)$$

where ϵ is the dimensionless softening parameter and $0 < \epsilon \ll 1$.

We use (x, y, z) to denote the standard Cartesian coordinates relative to which the node Ω and inclination I are measured. The total angular momentum is

$$\begin{aligned} \begin{pmatrix} L_x \\ L_y \\ L_z \end{pmatrix} &= \sum_{i=0}^{N-1} m_i \sqrt{GM_\bullet a_i} \begin{pmatrix} \sin I_i \sin \Omega_i \\ -\sin I_i \cos \Omega_i \\ \cos I_i \end{pmatrix} \\ &= \sum_{i=0}^{N-1} m_i \sqrt{GM_\bullet a_i} \begin{pmatrix} I_i \sin \Omega_i \\ -I_i \cos \Omega_i \\ 1 - \frac{1}{2} I_i^2 \end{pmatrix} + O(I_i^3) \\ &= \sum_{i=0}^{N-1} \begin{pmatrix} \gamma_i q_i \\ \gamma_i p_i \\ \gamma_i^2 - \frac{1}{2} q_i^2 - \frac{1}{2} p_i^2 \end{pmatrix} + O(I_i^3). \end{aligned} \quad (38)$$

It is straightforward to show that all three components of the total angular momentum are conserved (see discussion following eqs. 49–51).

The Hamiltonian can be rewritten as

$$H(\mathbf{q}, \mathbf{p}) = \mathbf{p}^T \mathbf{A} \mathbf{p} + \mathbf{q}^T \mathbf{A} \mathbf{q}, \quad (39)$$

where $\mathbf{p}^T = (p_0, \dots, p_{N-1})$, $\mathbf{q}^T = (q_0, \dots, q_{N-1})$ and the $N \times N$ matrix \mathbf{A} is defined by

$$\begin{aligned} A_{ij} &= -\frac{Gm_i m_j \alpha_{ij}}{8 \max(a_i, a_j) \gamma_i \gamma_j} b_{3/2}^{(1)}(\alpha_{ij}) & \text{if } i \neq j \\ &= \sum_{k \neq i} \frac{Gm_i m_k \alpha_{ik}}{8 \max(a_i, a_k) \gamma_i^2} b_{3/2}^{(1)}(\alpha_{ik}) & \text{if } i = j. \end{aligned} \quad (40)$$

Note that

$$\sum_{j=0}^{N-1} A_{ij} \gamma_j = 0. \quad (41)$$

Since \mathbf{A} is symmetric, it can be diagonalized in the form

$$\mathbf{A} = \mathbf{O} \mathbf{\Lambda} \mathbf{O}^T, \quad (42)$$

where \mathbf{O} is orthogonal ($\mathbf{O}^T = \mathbf{O}^{-1}$) and $\mathbf{\Lambda}$ is diagonal. The diagonal elements of $\mathbf{\Lambda}$ are the eigenvalues of \mathbf{A} and the columns of \mathbf{O} are the normalized eigenvectors (see Figures 3–4 below for properties of the eigenvalues and eigenvectors in simulated discs).

Now consider a canonical transformation to new coordinates and momenta (\mathbf{Q}, \mathbf{P}) having the generating function

$$S = \mathbf{P}^T \mathbf{O}^T \mathbf{q}. \quad (43)$$

Then

$$\mathbf{p} = \frac{\partial S}{\partial \mathbf{q}} = \mathbf{O} \mathbf{P}, \quad \mathbf{Q} = \frac{\partial S}{\partial \mathbf{P}} = \mathbf{O}^T \mathbf{q}, \quad \mathbf{q} = \mathbf{O} \mathbf{Q}, \quad (44)$$

and

$$H(\mathbf{P}, \mathbf{Q}) = \mathbf{P}^T \mathbf{\Lambda} \mathbf{P} + \mathbf{Q}^T \mathbf{\Lambda} \mathbf{Q}. \quad (45)$$

The inclinations of stars can be calculated from \mathbf{Q} and \mathbf{P} as

$$I_j^2 = \frac{q_j^2 + p_j^2}{\gamma_j^2} = \left(\sum_{i=0}^{N-1} \frac{O_{ji}}{\gamma_j} Q_i \right)^2 + \left(\sum_{i=0}^{N-1} \frac{O_{ji}}{\gamma_j} P_i \right)^2. \quad (46)$$

Since H is separable, $P_i^2 + Q_i^2$ is a constant of motion for all $i = 0, \dots, N-1$. The equations of motion are

$$\dot{Q}_i = \frac{\partial H}{\partial P_i} = 2\Lambda_i P_i, \quad \dot{P}_i = -\frac{\partial H}{\partial Q_i} = -2\Lambda_i Q_i, \quad (47)$$

which have the solution

$$\begin{aligned} Q_i(t) &= Q_i(0) \cos(2\Lambda_i t) + P_i(0) \sin(2\Lambda_i t), \\ P_i(t) &= -Q_i(0) \sin(2\Lambda_i t) + P_i(0) \cos(2\Lambda_i t). \end{aligned} \quad (48)$$

Thus Λ_i can be regarded as a frequency.

Since $b_{3/2}^{(1)}(\alpha)$ is positive, equation (32) implies that $H \geq 0$. Thus $H(\mathbf{q}, \mathbf{p})$ is a positive semi-definite quadratic form defined by the matrix \mathbf{A} , and thus all of the eigenvalues Λ_i are non-negative. The lower bound $H = 0$ is achieved if $p_i/\gamma_i = \text{const}$, $q_i/\gamma_i = \text{const}$ independent of i , corresponding to a uniform tilt of the disc plane. Thus there is one zero eigenvalue, which we call Λ_0 , and the rest are positive; in the discussions below we always order the eigenvectors by eigenvalue, so $\Lambda_0 = 0 < \Lambda_1 < \dots < \Lambda_{N-1}$. The eigenvector corresponding to zero eigenvalue is $c(\gamma_0, \dots, \gamma_{N-1})$ where c is a constant (cf. eq. 41). Since the columns of \mathbf{O} are normalized eigenvectors, $O_{j0} = c\gamma_j$ with $c = \pm(\sum_j \gamma_j^2)^{-1/2}$ and

$$\begin{aligned} Q_0 &= \sum_{j=0}^{N-1} O_{j0} q_j = c \sum_{j=0}^{N-1} \gamma_j q_j = cL_x, \\ P_0 &= \sum_{j=0}^{N-1} O_{j0} p_j = c \sum_{j=0}^{N-1} \gamma_j p_j = cL_y, \end{aligned} \quad (49)$$

where the last equalities follow from (38). Since $\Lambda_0 = 0$, P_0 and Q_0 are constant, so the x and y components of the total angular momentum are conserved, as they must be.

We define

$$Z(\mathbf{q}, \mathbf{p}) \equiv \sum_{i=0}^{N-1} (q_i^2 + p_i^2). \quad (50)$$

Following Laskar (2000), we call $\frac{1}{2}Z$ the ‘angular-momentum deficit’ since it represents the difference between the z component of the angular momentum of the actual system and the angular momentum that it would have if all of the stars were on coplanar circular orbits (eq. 38). Since the canonical transformation from (\mathbf{q}, \mathbf{p}) to (\mathbf{Q}, \mathbf{P}) is orthogonal

$$Z(\mathbf{Q}, \mathbf{P}) = \sum_{i=0}^{N-1} (Q_i^2 + P_i^2) = \mathbf{Q}^T \mathbf{Q} + \mathbf{P}^T \mathbf{P}. \quad (51)$$

Since $Q_i^2 + P_i^2$ is constant for all i , Z is also constant, which confirms that the z component of angular momentum is conserved, as it must be.

Normal modes that have wavelengths that are short compared to the disc radius but long compared to the radial separation between stars (roughly, $a \gg \lambda \gg a/N$ where a is the disc radius and N is the number of stars) approximately satisfy the WKB dispersion relation for bending waves (Hunter & Toomre 1969; Binney & Tremaine 2008)

$$(\omega - m\Omega)^2 = \nu^2 + (2\pi)^2 \frac{G\Sigma}{\lambda} \quad (52)$$

where ν is the vertical frequency arising from an external potential and m is the azimuthal wavenumber. In our case $m = 1$, $\nu = \Omega$, and $|\omega| \ll \Omega$, so the dispersion relation

simplifies to

$$\omega = -\frac{2\pi^2 G\Sigma}{\Omega\lambda}. \quad (53)$$

The n^{th} normal mode has approximately n nodes, and so the average wavelength of this mode is roughly $2(r_{\text{max}} - r_{\text{min}})/n$. The longest waves have the lowest frequencies, and the frequency of mode n is proportional to $\omega_n \propto n$, consistent with the low-frequency behavior seen in Figure 3 below.

4 INTERACTIONS BETWEEN THE DISC AND A SURROUNDING STELLAR SYSTEM

Let us suppose that there is an external perturbation to the disc, which can be represented by generalized forces f_{qi} , f_{pi} that change the coordinate and momentum of ring i at a rate $\dot{q}_i = f_{qi}$, $\dot{p}_i = f_{pi}$. Since $\gamma_i q_i$ and $\gamma_i p_i$ are the x and y components of the angular momentum of star i (cf. eq. 38) we have

$$f_{qi}(t) = \gamma_i^{-1} T_{xi}(t), \quad f_{pi}(t) = \gamma_i^{-1} T_{yi}(t) \quad (54)$$

where $T_{xi}(t)$, $T_{yi}(t)$ are the x and y components of the orbit-averaged external torque on star i . If these torques arise from a surrounding distribution of stars that is stationary and spherical on average, then $\langle f_{qi}(t) \rangle = \langle f_{pi}(t) \rangle = 0$ for all i where $\langle \cdot \rangle$ denotes an ensemble average over realizations of the surrounding stellar cluster. With the same assumptions we also have that $\langle f_{qi}(t) f_{pj}(t') \rangle = 0$ for all i and j . Since the number of stars in the surrounding cluster is large, $f_{qi}(t)$ and $f_{pi}(t)$ are Gaussian random processes. These can be uniquely characterized by the correlation coefficient

$$\Gamma_{ij}(t, t') \equiv \Gamma_{ij}(|t - t'|) \equiv \langle f_{qi}(t) f_{qj}(t') \rangle = \langle f_{pi}(t) f_{pj}(t') \rangle, \quad (55)$$

where the first and last equality are valid if the forces are stationary and spherically symmetric on average. Note that $\Gamma_{ij}(t)$ need not be diagonal since nearby stars are expected to experience similar torques. The coherence time τ of the external torques is defined so that

$$\Gamma_{ij}(\Delta t) \simeq 0 \quad \text{for } |\Delta t| \gtrsim \tau. \quad (56)$$

In the next two subsections, we discuss the general properties of the growth of perturbations from an initially thin coplanar disc, then we construct a specific model for the torques and correlations.

4.1 Response of the disc to external torques

The equations of motion (47) in the canonical coordinates (\mathbf{Q}, \mathbf{P}) are modified to

$$\dot{Q}_i = 2\Lambda_i P_i + \sum_{j=0}^{N-1} O_{ji} f_{qj}(t), \quad \dot{P}_i = -2\Lambda_i Q_i + \sum_{j=0}^{N-1} O_{ji} f_{pj}(t). \quad (57)$$

Let us assume that the modes of the disc are non-degenerate, that is, $\Lambda_i = \Lambda_j$ only if $i = j$ (this is not an important restriction for practical purposes). With the initial conditions

$Q_i(0) = P_i(0) = 0$, equations (57) have the solution

$$\begin{aligned} Q_i(t) &= \sum_{j=0}^{N-1} O_{ji} \int_0^t dt_1 \{ f_{qj}(t_1) \cos[2\Lambda_i(t - t_1)] \\ &\quad + f_{pj}(t_1) \sin[2\Lambda_i(t - t_1)] \} \\ P_i(t) &= \sum_{j=0}^{N-1} O_{ji} \int_0^t dt_1 \{ f_{pj}(t_1) \cos[2\Lambda_i(t - t_1)] \\ &\quad - f_{qj}(t_1) \sin[2\Lambda_i(t - t_1)] \}. \end{aligned} \quad (58)$$

The mean squared value of the process over different realizations of the perturbing torques is

$$\begin{aligned} \langle Q_i^2(t) \rangle &= \langle P_i^2(t) \rangle \\ &= \sum_{n,m=0}^{N-1} O_{ni} O_{mi} \int_0^t dt_1 \int_0^t dt_2 \\ &\quad \times \{ \langle f_{qn}(t_1) f_{qm}(t_2) \rangle \cos[2\Lambda_i(t - t_1)] \cos[2\Lambda_i(t - t_2)] \\ &\quad + \langle f_{pn}(t_1) f_{pm}(t_2) \rangle \sin[2\Lambda_i(t - t_1)] \sin[2\Lambda_i(t - t_2)] \} \\ &= \sum_{n,m=0}^{N-1} O_{ni} O_{mi} \int_0^t dt_1 \int_0^t dt_2 \Gamma_{nm}(t_2 - t_1) \cos[2\Lambda_i(t_2 - t_1)] \\ &= 2 \sum_{n,m=0}^{N-1} O_{ni} O_{mi} \int_0^t dt' (t - t') \Gamma_{nm}(t') \cos 2\Lambda_i t' \end{aligned} \quad (59)$$

where in the second-last line we have used the definition of $\Gamma_{nm}(t)$ (eq. 55) and the trigonometric identity for the sum of cosines, and in the last line we have used $\Gamma_{nm}(t) = \Gamma_{nm}(-t)$. Note also that

$$\langle Q_i(t) P_i(t) \rangle = 0. \quad (60)$$

Similarly, we can calculate the cross-correlation coefficient between two modes with $\Lambda_i \neq \Lambda_j$,

$$\begin{aligned} \langle Q_i(t) Q_j(t) \rangle &= \langle P_i(t) P_j(t) \rangle \\ &= \sum_{n,m=0}^{N-1} O_{ni} O_{mj} \int_0^t dt_1 \int_0^t dt_2 \\ &\quad \times \{ \langle f_{qn}(t_1) f_{qm}(t_2) \rangle \cos[2\Lambda_i(t - t_1)] \cos[2\Lambda_j(t - t_2)] \\ &\quad + \langle f_{pn}(t_1) f_{pm}(t_2) \rangle \sin[2\Lambda_i(t - t_1)] \sin[2\Lambda_j(t - t_2)] \} \\ &= \sum_{n,m=0}^{N-1} O_{ni} O_{mj} \int_0^t dt_1 \int_0^t dt_2 \\ &\quad \times \Gamma_{nm}(t_2 - t_1) \cos[2\Lambda_i(t - t_1) - 2\Lambda_j(t - t_2)] \\ &= \sum_{n,m=0}^{N-1} O_{ni} O_{mj} \frac{\cos(\Delta_{ij} t)}{\Delta_{ij}} \int_0^t dt' \Gamma_{nm}(t') \\ &\quad \times [\sin(\Delta_{ij} t - 2\Lambda_i t') + \sin(\Delta_{ij} t + 2\Lambda_j t')] \end{aligned} \quad (61)$$

where we have introduced $\Delta_{ij} = \Lambda_i - \Lambda_j$ to simplify notation.

A similar calculation shows that

$$\langle Q_i(t) P_j(t) \rangle = \tan(\Delta_{ij} t) \langle Q_i(t) Q_j(t) \rangle. \quad (62)$$

The mean squared inclinations at time t follow from equations (46), (59), and (61),

$$\langle I_j^2(t) \rangle = \sum_{k,l=0}^{N-1} \frac{O_{jk} O_{jl}}{\gamma_j^2} [\langle Q_k(t) Q_l(t) \rangle + \langle P_k(t) P_l(t) \rangle] \quad (63)$$

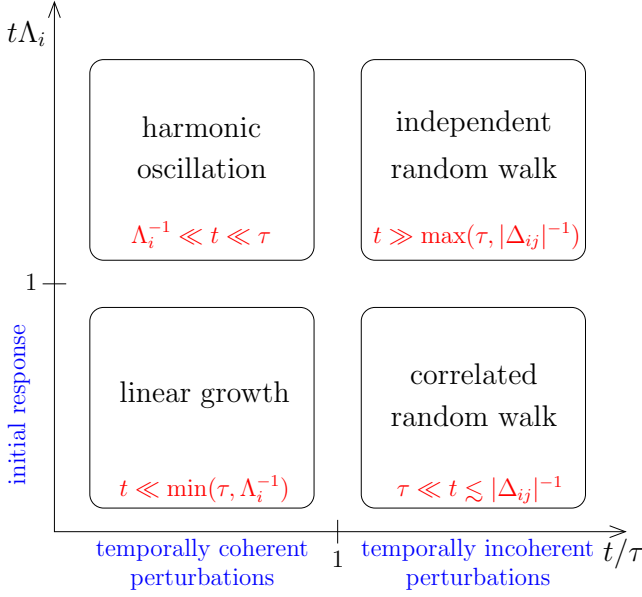


Figure 2. Evolutionary stages of the excitation of normal modes of an initially thin, flat stellar disc by stochastic external perturbations. On the horizontal axis, the age of the disc t is measured relative to τ , the coherence time of the perturbations. The vertical axis shows t relative to the inverse frequencies Λ_i^{-1} of the normal modes of the disc. If $t \ll \tau$ the perturbations are temporally coherent, and the normal mode amplitudes initially grow linearly, then saturate and oscillate with angular frequency $2\Lambda_i$. For $t \gg \tau$ the perturbations are temporally incoherent, and the amplitudes of modes i and j undergo initially correlated, later independent, random walks (before and after time $|\Delta_{ij}^{-1}| = |\Lambda_i - \Lambda_j|^{-1}$, respectively). The evolution in these regimes is examined separately in §4.1.1, 4.1.2, and 4.1.3.

In the rest of this paper we explore the implications of equations (57)–(63) for the evolution of an initially planar disc excited by stochastic torques. First, we make general statements, then we examine applications to the Galactic-centre disc(s) in the next section.

These equations contain three characteristic time-scales: (i) the age of the disc t , which determines the interval over which the external torques have acted on the initially thin and flat disc; (ii) the inverse frequencies Λ_i^{-1} of the normal modes of the disc; (iii) the coherence time τ of the perturbations (eq. 56).

Note that any perturbation that is initially zero, and then grows and decays smoothly with coherence time τ (i.e., a perturbation whose temporal power spectrum contains only frequencies $\gtrsim 1/\tau$) cannot excite short-period normal modes ($\Lambda_i^{-1} \ll \tau$) because the actions and hence amplitudes of these modes are adiabatic invariants (an analogy arises in the disruption of open clusters by molecular clouds: the tidal forces from the clouds are ineffective if the orbital period of the stars in the cluster is small compared to the passage time; see Spitzer 1958).

The time evolution of the disc can be understood analytically in the following limiting cases, shown schematically in Figure 2.

4.1.1 Initial response, $t \ll \Lambda_i^{-1}$

When the age of the disc is much less than the inverse frequency of a particular normal mode i , the factor $\cos 2\Lambda_i t'$ in the integrand of equation (59) is unity and we have

$$\langle Q_i^2 \rangle = \langle P_i^2 \rangle = 2 \sum_{n,m=0}^{N-1} O_{ni} O_{mi} \int_0^t dt' (t-t') \Gamma_{nm}(t'). \quad (64)$$

In particular, the zero-frequency ($i = 0$) normal mode describing the mean orientation of the disc (cf. eq. 49) always grows according to equation (64).

If the disc age is much smaller than Λ_i^{-1} for *all* modes i , then equation (61) yields

$$\langle Q_i Q_j \rangle = \langle P_i P_j \rangle = 2 \sum_{n,m=0}^{N-1} O_{ni} O_{mj} \int_0^t dt' (t-t') \Gamma_{nm}(t'). \quad (65)$$

and the orthogonal transformation to (q_i, p_i) yields

$$\langle q_i^2 \rangle = \langle p_i^2 \rangle = 2 \int_0^t dt' (t-t') \Gamma_{ii}(t'), \quad \text{if } t \ll \min_i \Lambda_i^{-1}. \quad (66)$$

(The same result would obtain if the disc mass were small enough that the collective effects from its self-gravity were negligible.) The inclination distribution is given by equation (46),

$$\langle I_j^2 \rangle = \frac{4}{\gamma_j^4} \int_0^t dt' (t-t') \langle T_{xj}(0) T_{xj}(t') \rangle, \quad t \ll \min_i \Lambda_i^{-1}. \quad (67)$$

4.1.2 Temporally coherent perturbations, $t \ll \tau$

When the disc age t is much shorter than the coherence time τ , the external forces are approximately constant over the lifetime of the disc, so $\Gamma_{jk}(t) \simeq \text{const}$, and equations (59) and (61) simplify to

$$\begin{aligned} \langle Q_i^2 \rangle = \langle P_i^2 \rangle &= \sum_{n,m=0}^{N-1} O_{ni} O_{mi} \Gamma_{nm} \frac{\sin^2 \Lambda_i t}{\Lambda_i^2}, \\ \langle Q_i Q_j \rangle = \langle P_i P_j \rangle &= \sum_{n,m=0}^{N-1} O_{ni} O_{mj} \Gamma_{nm} \frac{\sin \Lambda_i t \sin \Lambda_j t}{\Lambda_i \Lambda_j} \cos \Delta_{ij} t. \end{aligned} \quad (68)$$

Initially, the amplitude of each normal mode grows linearly with time with a rate independent of Λ_i . Then after a saturation time $t_{s,i} \equiv \frac{1}{2}\pi/\Lambda_i$ the amplitude reaches a maximum and begins to oscillate. At much larger times the time-averaged mean-square amplitude is $\langle Q_i^2 \rangle = \frac{1}{2} \sum_{nm} O_{ni} O_{mi} \Gamma_{nm} / \Lambda_i^2$.

The time evolution for any particular realization of the perturbing forces can be obtained directly from equation (58) by specializing to constant f_{qj} and f_{pj} ,

$$\begin{aligned} Q_i(t) &= \sum_{j=0}^{N-1} \frac{O_{ji}}{2\Lambda_i} [f_{qj} \sin 2\Lambda_i t - f_{pj} (\cos 2\Lambda_i t - 1)], \\ P_i(t) &= \sum_{j=0}^{N-1} \frac{O_{ji}}{2\Lambda_i} [f_{pj} \sin 2\Lambda_i t + f_{qj} (\cos 2\Lambda_i t - 1)] \end{aligned} \quad (69)$$

for $i > 0$ ($\Lambda_i \neq 0$); otherwise for $i = 0$ ($\Lambda_0 = 0$)

$$Q_0(t) = t \sum_{j=0}^{N-1} O_{j0} f_{qj}, \quad P_0(t) = t \sum_{j=0}^{N-1} O_{j0} f_{pj}. \quad (70)$$

4.1.3 Temporally incoherent perturbations, $t \gg \tau$.

When the disc age is much larger than the coherence time, then since $\Gamma_{nm}(t') = 0$ for $t' \gtrsim \tau$, the upper limit of the integration in equations (59) and (61) can be truncated at τ , so

$$\begin{aligned} \langle Q_i^2(t) \rangle &= \langle P_i^2(t) \rangle = g_i t - h_i, \quad \text{if } t \gtrsim \tau, \quad (71) \\ \langle Q_i(t) Q_j(t) \rangle &= \frac{\cos \Delta_{ij} t}{\Delta_{ij}} [A_{ij} \cos \Delta_{ij} t + B_{ij} \sin \Delta_{ij} t], \\ \langle Q_i(t) P_j(t) \rangle &= \frac{\sin \Delta_{ij} t}{\Delta_{ij}} [A_{ij} \cos \Delta_{ij} t + B_{ij} \sin \Delta_{ij} t], \end{aligned}$$

where the constants A_{ij} , B_{ij} , g_i , and h_i are

$$\begin{aligned} A_{ij} &= \sum_{n,m=0}^{N-1} O_{ni} O_{mj} \int_0^\tau dt' \Gamma_{nm}(t') [\sin(2\Lambda_j t') - \sin(2\Lambda_i t')] \\ B_{ij} &= \sum_{n,m=0}^{N-1} O_{ni} O_{mj} \int_0^\tau dt' \Gamma_{nm}(t') [\cos(2\Lambda_i t') + \cos(2\Lambda_j t')] \\ g_i &= B_{ii}, \quad h_i = 2 \sum_{n,m=0}^{N-1} O_{ni} O_{mi} \int_0^\tau dt' t' \Gamma_{nm}(t') \cos 2\Lambda_i t'. \end{aligned} \quad (72)$$

For $t \gg \max(\tau, h_i/g_i)$, $\langle Q_i^2(t) \rangle = \langle P_i^2(t) \rangle \simeq g_i t$; moreover $\langle Q_i(t) P_i(t) \rangle = 0$ (eq. 60), and $\langle Q_i(t) Q_j(t) \rangle$ and $\langle Q_i(t) P_j(t) \rangle$ are bounded by $\pm \sqrt{A_{ij}^2 + B_{ij}^2}/|\Delta_{ij}|$, so after $t \gg \max[\tau, |\Delta_{ij}|^{-1}(A_{ij}^2 + B_{ij}^2)^{1/2}/g_i]$, the cross-correlation becomes negligible compared to $\langle Q_i^2(t) \rangle$. In other words, at large times $Q_i(t)$ and $P_i(t)$ undergo random walks. The random walks of various modes i and j are first correlated then gradually become independent after the disc lifetime becomes much larger than the inverse relative normal mode frequencies $|\Delta_{ij}|^{-1}$.

In our case none of these simple limits applies: the coherence time of the perturbations from the cluster is the vector resonant relaxation time-scale, and this can be shorter or longer than the disc age depending on the radius and the effective mass m_2 in the cluster (cf. Fig. 1). Moreover the set of inverse frequencies Λ_i^{-1} includes values that are both shorter and longer than the disc age (Fig. 3). We compare these time-scales numerically for Monte Carlo simulations of the stellar disc in §5 below.

Finally, the configuration of an isolated disc in thermal equilibrium under vector resonant relaxation is discussed in the Appendix.

4.2 Distribution of torques

We now construct a model for the perturbing torques $\{T_{xi}, T_{yi}\}$. These are the sum of the torques from all of the stars in the cluster on the disc star labelled by i , in a circular orbit near the $z = 0$ plane; the torques are averaged over the orbit of both the cluster star and the disc star. To simplify the calculation at modest cost in realism, we assume that the cluster stars are also on circular orbits. Then the total torque on disc stars on circular orbits can be calculated from the gravitational torque acting between circular rings

or wires of uniform density:

$$\mathbf{T}_i = \sum_{\beta} \sum_{\ell=1}^{\infty} K_{i\beta\ell} P'_{2\ell}(\mathbf{n}_{\beta} \cdot \mathbf{n}_i) \mathbf{n}_i \times \mathbf{n}_{\beta}, \quad (73)$$

where i and β label disc and cluster stars, respectively, \mathbf{L}_i or \mathbf{L}_{β} is the angular momentum vector of star i or β , and $\mathbf{n}_{\beta} = \mathbf{L}_{\beta}/|\mathbf{L}_{\beta}|$ is the unit vector aligned with the angular momentum, which is related to the node Ω_{β} and inclination I_{β} by $\mathbf{n}_{\beta} = (\sin I_{\beta} \sin \Omega_{\beta}, -\sin I_{\beta} \cos \Omega_{\beta}, \cos I_{\beta})$. We also have

$$K_{i\beta\ell} = G m_i m_{\beta} [P_{2\ell}(0)]^2 \frac{r_{i\beta <}^{2\ell}}{r_{i\beta >}^{2\ell+1}}, \quad P_{2\ell}(0) = \frac{(-1)^{\ell} \Gamma(2\ell+1)}{2^{2\ell} \Gamma^2(\ell+1)}. \quad (74)$$

Here m_{β} and r_{β} are the mass and orbital radius of star β (recall that both the disc and cluster stars are assumed to be on circular orbits), $r_{i\beta <} = \min(r_i, r_{\beta})$, $r_{i\beta >} = \max(r_i, r_{\beta})$, and $P_{2\ell}(x)$ and $P'_{2\ell}(x)$ are the Legendre polynomial and its first derivative¹¹. The sum over ℓ in equation (73) is absolutely convergent unless $r_i = r_{\beta}$. The analytical formula (29) for the precession rate when $r_{<}/r_{>} \ll 1$ is the corresponding limiting case of equation (73).

In the discussions below, we neglect the back-reaction of the disc stars on the orbits of stars in the old cluster. This approximation should be valid so long as the total angular momentum contained in the fluctuating non-spherical component of the star cluster exceeds the angular momentum in the disc. The former is roughly $N^{1/2} m_2 (GM_{\bullet} r)^{1/2}$ where $m_2 = \langle m^2 \rangle / \langle m \rangle$ is the effective mass and $N = M(r)/m_2$ is the effective number of stars in the cluster at radius r ; the latter is $M_{\text{disc}} (GM_{\bullet} r)^{1/2}$. Thus the neglect of the back-reaction should be valid so long as $[M(r) m_2]^{1/2} \gtrsim M_{\text{disc}}$. This is the same as the criterion that nodal precession is dominated by the stochastic field from the old cluster rather than the disc, as discussed following equation (26).

Assuming that the disc is flat (i.e., zero inclination for all disc stars), equation (73) simplifies to

$$\begin{pmatrix} T_{xi} \\ T_{yi} \end{pmatrix} = \sum_{\beta} \sum_{\ell=1}^{\infty} K_{i\beta\ell} P_{2\ell}^1(\cos I_{\beta}) \begin{pmatrix} \cos \Omega_{\beta} \\ \sin \Omega_{\beta} \end{pmatrix}. \quad (75)$$

4.2.1 The torques as a Gaussian random process

In a spherical cluster, or the equatorial plane of an axisymmetric cluster, the torques described by equation (75) are the sum of a large number of independent random variables with zero mean. Hence, according to the central limit theorem, the probability distribution of the torques T_{xi} and T_{yi} is Gaussian, with zero mean and covariance or correlation function $\langle T_{xi}(0) T_{xj}(t) \rangle = \langle T_{yi}(0) T_{yj}(t) \rangle = \gamma_i \gamma_j \Gamma_{ij}(t)$. From equation (75) it is also clear that $\langle T_{xi} T_{yj} \rangle = 0$ in a spherical cluster, for all i and j .

A Gaussian random process is fully characterised by its mean and correlation function. Thus, when generating a Monte Carlo distribution of cluster stars, the distribution of torques is the same for all mass functions having the same effective mass m_2 so long as the total mass distribution $M(r)$

¹¹ In terms of the associated Legendre function $P_n^m(x)$, $P'_{2\ell}(\cos I) = -P_{2\ell}^1(\cos I)/\sin I$.

is fixed. Thus we may assume without loss of generality that all the cluster stars have mass $m_\beta = m_2$.

Next we examine the spatial correlation function of cluster torques $\langle T_{xi}(0)T_{xj}(0) \rangle = \gamma_i \gamma_j \Gamma_{ij}(0)$. We are mostly interested here in the correlation function within a thin, flat disc. Then we may use equation (75) for the torques, which yields

$$\begin{aligned} & \langle T_{xi}(0)T_{xj}(0) \rangle \\ &= \left\langle \sum_{\beta, \ell, \ell'} K_{i\beta\ell} K_{j\beta\ell'} P_{2\ell}^1(\cos I_\beta) P_{2\ell'}^1(\cos I_\beta) \sin^2 \Omega_\beta \right\rangle \\ &= G^2 m_i m_j \sum_\beta m_\beta^2 \sum_{\ell=1}^{\infty} [P_{2\ell}(0)]^2 k_\ell \frac{r_{i\beta}^{2\ell} < r_{j\beta}^{2\ell}}{r_{i\beta}^{2\ell+1} r_{j\beta}^{2\ell+1}}, \end{aligned} \quad (76)$$

where k_ℓ is a constant defined as

$$\begin{aligned} k_\ell &= [P_{2\ell}(0)]^2 \langle P_{2\ell}^1(\cos I_\beta) P_{2\ell}^1(\cos I_\beta) \rangle \langle \sin^2 \Omega_\beta \rangle \\ &= \frac{2\ell(1+2\ell) \Gamma^2(\ell+1/2)}{\pi(1+4\ell) \Gamma^2(\ell+1)}. \end{aligned} \quad (77)$$

Here we have used the orthogonality of the Legendre functions, $\langle P_{2\ell}^m(\cos I_\beta) P_{2\ell'}^m(\cos I_\beta) \rangle = 0$ for $\ell \neq \ell'$.

We have separated k_ℓ from the factor $[P_{2\ell}(0)]^2$ in equation (76) because k_ℓ is practically independent of ℓ ; as ℓ varies from 1 to ∞ , k_ℓ varies only from $3/10 = 0.3$ to $1/\pi = 0.3183$. Therefore we can estimate the correlation function to reasonable accuracy by replacing k_ℓ with a constant k , $0.3 \leq k < 0.32$. This leads to a power series in ℓ which is reminiscent of the power series defining the complete elliptic integral of the first kind, $K(x) = \frac{1}{2}\pi \sum_{n=0}^{\infty} [P_{2n}(0)]^2 x^{2n}$. Therefore

$$\begin{aligned} & \langle T_{xi}(0)T_{xj}(0) \rangle \\ &= G^2 k m_i m_j \sum_\beta \frac{m_\beta^2}{r_{i\beta} > r_{j\beta} >} \left[\frac{2}{\pi} K(\alpha_{i\beta} \alpha_{j\beta}) - 1 \right], \end{aligned} \quad (78)$$

where $\alpha_{i\beta} = r_{i\beta} < / r_{i\beta} > = \min(r_i, r_\beta) / \max(r_i, r_\beta)$. We may express this result in terms of the density of the cluster $\rho(r)$ (eq. 7) and the effective mass $m_2 = \langle m_\beta^2 \rangle / \langle m_\beta \rangle$,

$$\begin{aligned} & \langle T_{xi}(0)T_{xj}(0) \rangle = 4\pi G^2 k m_i m_j m_2 \\ & \times \int_0^\infty \frac{dr r^2 \rho(r)}{\max(r, r_i) \max(r, r_j)} \left[\frac{2}{\pi} K(\alpha_i \alpha_j) - 1 \right], \end{aligned} \quad (79)$$

where $\alpha_i = \min(r, r_i) / \max(r, r_i)$.

Equations (78)–(79) define the probability density of torques acting on the disc stars at each instant. They show that the correlation function for disc stars at radii r_i and r_j is determined mainly by cluster stars in the region $\min(r_i, r_j) \lesssim r \lesssim \max(r_i, r_j)$. In particular, at large radii $\rho(r) \propto r^{-1.75}$ (eq. 7) so for $r \gg \max(r_i, r_j)$ the integrand declines as $r_i^2 r_j^2 r^{-5.75}$, so the contribution to the correlation function from this region is negligible. At small radii, $\rho(r) \propto r^{-1.2}$ so for $r \ll \min(r_i, r_j)$ the integrand scales as $r^{4.2} / (r_i^3 r_j^3)$, implying that the contribution from small radii is also negligible. Gürkan & Hopman (2007) reach a similar conclusion.

A simple fitting formula for equation (79), using the mass distribution in the Galactic centre (eq. 8), is

$$\langle T_{xi}(0)T_{xj}(0) \rangle \simeq c_T \frac{m_2 \rho(\bar{r}_{ij}) \bar{r}_{ij}^3}{M_\bullet^2} L_i L_j \Omega(r_i) \Omega(r_j) \alpha_{ij}^\kappa \quad (80)$$

where $\alpha_{ij} = \min(r_i, r_j) / \max(r_i, r_j)$, $\bar{r}_{ij} = \sqrt{r_i r_j}$, $L_i = m_i r_i^2 \Omega(r_i)$ is the angular momentum, and c_T and κ are fit parameters. The best fit values, which approximate equation (79) to better than 20% over radii $\alpha_{ij} < 4$ and $\bar{r}_{ij} < 4$ pc, are $c_T = 0.77$ and $\kappa = 1.8$. Thus, the correlation of torques on different stars, $\langle T_{xi} T_{xj} \rangle / [\langle T_{xi}^2 \rangle^{1/2} \langle T_{xj}^2 \rangle^{1/2}]$, is less than 14% for $a_i \geq 3a_j$. Furthermore, the distribution of torques is a smooth function of radii with a peak at $a_i = a_j$.

5 MONTE CARLO SIMULATIONS

We construct a flat, razor-thin disc of N stars on circular orbits. The disc is assumed to lie initially in the reference plane so $I_i = q_i / \gamma_i = p_i / \gamma_i = 0$, for all $i = 0, \dots, N-1$. The semi-major axes are chosen randomly from the surface density distribution (1) with exponent $\delta = 1.4$ (Bartko et al. 2010), between inner and outer radii of 0.04 and 0.6 pc (roughly 1 arcsec to 15.5 arcsec). The stellar masses are chosen from the mass function (14) with $\alpha = -0.45$, $m_{\max} = 30 M_\odot$ and $m_{\min} = 1 M_\odot$; the minimum mass is arbitrary but this choice has almost no influence on our results, and the maximum is the most massive star that can survive for the 6 Myr age of the disc(s) (Lejeune & Schaerer 2001). We set the total number of stars to be 500 in this mass range, implying that ~ 120 stars have masses $M \geq 20 M_\odot$, consistent with observations – 90 massive WR/O stars have been observed with $\sim 75\%$ spectroscopic completeness (Bartko et al. 2009), and these typically have masses $m > 20 M_\odot$ (Paumard et al. 2006). The corresponding disc mass is $6.3 \times 10^3 M_\odot$.

5.1 Normal modes

As discussed above, the evolution of the disc is most easily described in terms of its normal modes. We generate 1000 Monte Carlo realizations of the disc (stellar masses and semi-major axes). For each realization, we calculate the matrices \mathbf{A} and \mathbf{O} (eqs. 40 and 42), as well as the eigenvectors (the columns of \mathbf{O}). As explained in §4.1, the evolution of the disc is determined by the relation between three characteristic time-scales: the inverse normal mode frequencies Λ_i^{-1} , the coherence time τ of torques from the spherical cluster, and the age of the disc t .

Figure 3 shows the distribution of the saturation time $t_{s,i} = \frac{1}{2}\pi / \Lambda_i$, the characteristic time-scale at which the amplitude of a mode subjected to a fixed torque stops growing and begins to oscillate (see §4.1.2). The bottom (blue) curves show the mean distribution and the 95% confidence interval for our standard disc model. The figure shows that all but a few modes satisfy $t_{s,i} < 6$ Myr, and so are already saturated at the current age of the disc.

Some sample normal modes are shown in Figure 4. The height of the orbit of star j above the reference plane at azimuth ϕ is $z_j = r_j I_j \sin(\phi - \Omega_j) = -\gamma_j^{-1} r_j (q_j \cos \phi + p_j \sin \phi)$. Thus if only normal mode i is present, with amplitude (Q_i, P_i) , the height is $z_j = -r_j (Q_j \cos \phi + P_j \sin \phi) O_{ji} / \gamma_j$. The figure plots O_{ji} / γ_j which is proportional to the fractional height z_j / r_j at fixed azimuth. The left panel shows a single realization of our standard disc model and the centre panel shows an average over 1000 realizations. The modes are ordered by increasing frequency; mode $i = 0$ (the black

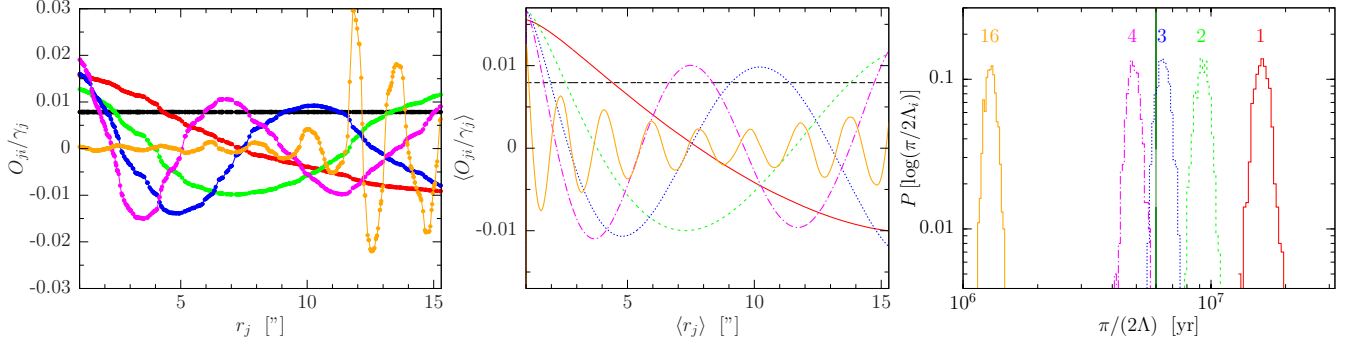


Figure 4. Normal modes of the stellar disc $i = 0, 1, 2, 3, 4$, and 16 (ordered by increasing frequency) for a randomly chosen realization (*left*), and averaged over 1000 realizations of the disc (*middle*). The vertical axis is proportional to the fractional height of the mode or the inclination angle at fixed azimuth. These modes of the stellar disc oscillate independently in the absence of the cluster. *Right*: Probability distribution of the saturation times for the same modes. A vertical green line shows the disc age $t = 6$ Myr. The models contain 500 disc stars with masses between $1 M_{\odot}$ and $30 M_{\odot}$ and radii between 1 arcsec and 30 arcsec.

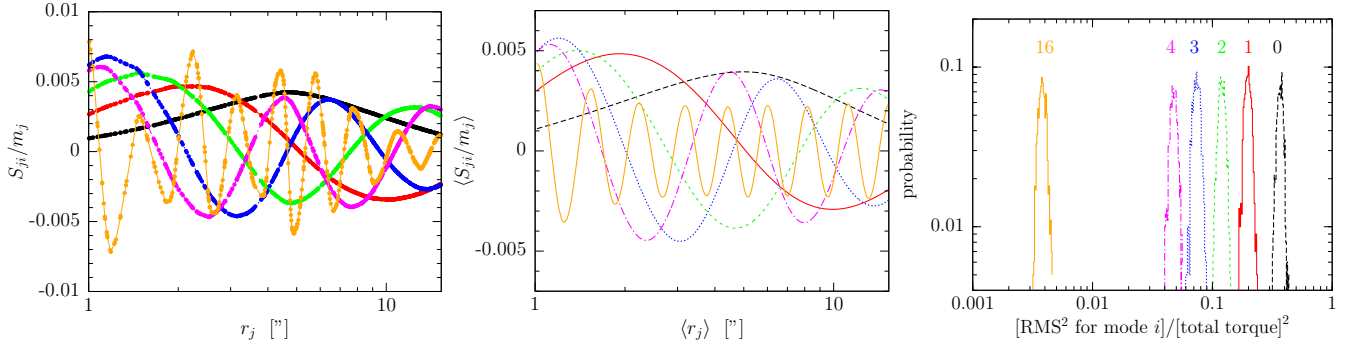


Figure 5. Driving modes of the spherical cluster, i.e., the eigenvectors of the spatial correlation function of the torques on the disc, $\langle T_{xi} T_{xj} \rangle$. The figure shows modes $i = 0, 1, 2, 3, 4$, and 16 (ordered by decreasing significance) for a randomly chosen realization (*left*), and averaged over 1000 realizations of the disc (*middle*). The models contain the same stars as in Fig. 4. *Right*: Probability distribution of the mean squared amplitude for the same modes.

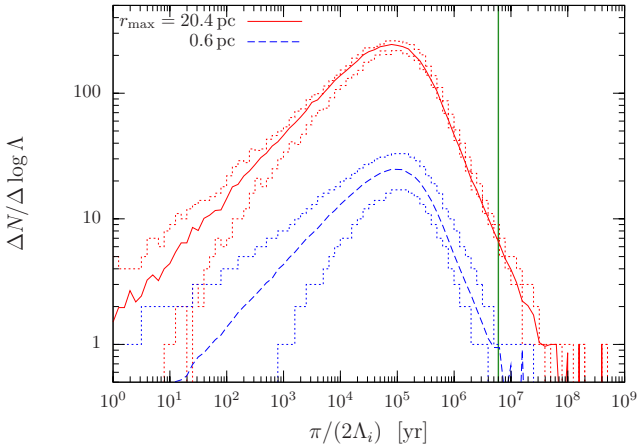


Figure 3. Histogram of saturation time-scales $\frac{1}{2}\pi/\Lambda_i$ for a disc of stars distributed between 1 arcsec and 15.5 arcsec (dashed blue) or extrapolated to 525 arcsec (solid red) with surface density $\Sigma(r) \propto r^{-1.4}$. The stellar masses are chosen from equation (14) with $\alpha = -0.45$, $m_{\max} = 30 M_{\odot}$, and $m_{\min} = 1 M_{\odot}$; the total number of stars is 500 and 5000 in the two cases. Dotted lines show the 95% confidence interval. The peak of the distribution corresponds to eigenmodes with average wavelengths comparable to the average distance between neighbouring stars. The age of the disc(s) in the Galactic center is marked by a vertical green line.

horizontal line in the figure) has frequency $\Lambda_0 = 0$ (eq. 49), and corresponds to a uniform tilt of the disc.

The low-frequency modes are rather smooth, and their shapes are approximately the same in different realizations of the disc – the mode shapes are not sensitive to the large random variations in the masses of individual stars ($1 M_{\odot} \leq m_j \leq 30 M_{\odot}$). The long-wavelength modes are well represented by the average waveform, while shorter wavelength modes in a single realization deviate more strongly from the mean (compare the orange lines, $i = 16$, in the left and centre panels of Figure 4). The right panel shows the probability distribution for the saturation times $\frac{1}{2}\pi/\Lambda_i$ for various realizations of the disc. The probability distribution is sharply peaked for Λ_i (for each fixed i) with a FWHM of about 20%. Therefore, Λ_i can be predicted from the surface-density distribution without knowing the locations and masses of disc stars. The normal modes $i = 0, 1, 2$ are still growing ($t_{s,i} > 6$ Myr), $i = 3$ is just around saturation, and all other modes are saturated.

These considerations and the theory presented in §4.1.2 allow us to make general remarks on the expected warping of the disc. Recall that modes in the oscillating phase – with either the coherence time or the disc age less than the saturation time $t_{s,i} = \frac{1}{2}\pi/\Lambda_i$ – are suppressed in amplitude relative to lower frequency modes by Λ_i^{-1} (see eq. [68] and

§5.3 below). Therefore if the external torques on the disc stars do not depend too strongly on radius, the shape of the disc is expected to be dominated by long-wavelength modes.

There are presently few observational constraints on the maximum radial extent of the disc, and its evolution would be different if it extended to larger radii. As an example, the top (red) curves in Figure 3 show the histogram of saturation times for a hypothetical disc extrapolated to 20.4 pc with the same power-law surface density distribution. In this case, there are many more modes still in the growing phase at the current age of 6 Myr. However, the characteristic wavelengths of these additional modes are larger than 0.6 pc, and the saturation timescales of the smaller wavelength modes are not very different from the case in which the disc is truncated at 0.6 pc. Therefore we expect that our predictions of the shape of the warped disc at radii $\lesssim 0.5$ pc are robust, and independent of whether or not there is an outer disc.

5.2 Spherical cluster

We model the torques on the disc from the star cluster as follows: (i) As described above, since the torque distribution is a Gaussian random process, we may assume that all cluster stars have the effective mass m_2 , as defined following equation (13); we typically assume $m_2 = 10 M_\odot$. (ii) As described above, for the sake of simplicity we assume that the cluster stars are on circular orbits, and generate a distribution of orbital radii consistent with the mass distribution $M(r)$ in equation (8) out to a radius of 2 pc, sufficiently far outside the disc(s) that the perturbations from larger radii should be small. (iii) We assign nodes Ω_β uniformly random between 0 and 2π and inclinations I_β so that $\cos I_\beta$ is uniformly random between -1 and $+1$, consistent with an isotropic distribution of orbits. (iv) We expand the torque (73) to order $2\ell = 10$. (v) We assume a disc age of 6 Myr.

Alternatively, random realizations of cluster torques may be generated by sampling an N -dimensional Gaussian distribution (where N is the number of disc stars) with a covariance matrix $\langle T_{xi} T_{xj} \rangle$ given by equations (79)–(80). We can decompose the torques into independent driving modes, corresponding to the eigenvectors of $\langle T_{xi} T_{xj} \rangle$. These driving modes, shown in Figure 5, are a property of the spherical cluster of old stars and hence are distinct from the normal modes of the disc shown in Figure 4. We find that the corresponding eigenvalues, which correspond to the mean squared amplitude of the particular driving mode, span a vast range, some 6 orders of magnitude. Remarkably, the five longest wavelength driving modes typically contribute 90% of the total torque. Therefore, the cluster excites the disc predominantly through a few long-wavelength driving modes.

As described at the end of §4.1.3, the coherence time of the torques from the cluster can be shorter than the disc age depending on the radius. The two are equal at a radius around $r_\tau \sim 0.3 \text{ pc} (m_2/10 M_\odot)^{0.56}$. Nevertheless, to avoid excessive complication – both conceptual and numerical – in our simulations we shall assume that the coherence time is long compared to the disc age, so that the perturbing forces $f_{qi}(t)$, $f_{pi}(t)$ can be regarded as time-independent and the formulae in §4.1.2 can be used to calculate the disc evolution. This simplification has a smaller impact on the evolution of long wavelength modes $\lambda \gtrsim r_\tau$, while it may be important

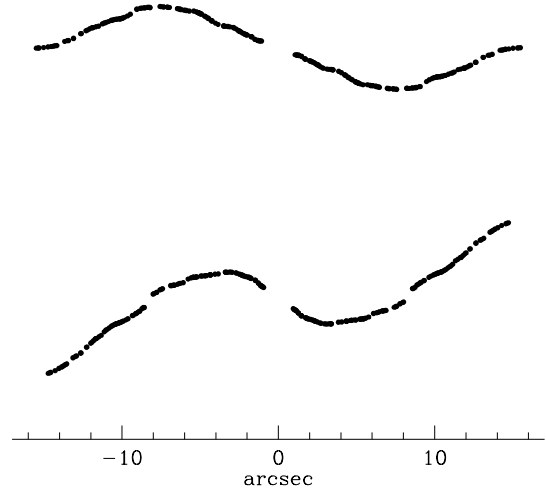


Figure 6. Two orthogonal cross-sections of a disc subjected to vector resonant relaxation. The parameters of the disc and the stellar cluster in which it is embedded are described in §5. The disc was initially horizontal. The calculation is based on the assumption that the inclinations are small and the results presented here are large enough that this approximation is not quantitatively accurate. Only stars with mass $> 20 M_\odot$ are shown but the stars of lower mass have the same thin, warped distribution. The simulation assumes that the disc age $t = 6$ Myr and the effective mass in the stellar cluster is $m_2 = 10 M_\odot$; the inclinations scale as $m_2^{1/2}$.

for short wavelength modes close to the center. To account properly for the temporal evolution of the torques from the cluster would require solving simultaneously for the secular evolution of both the cluster and the disc stars (see §6).

5.3 Warped disc

The results of a typical simulation are shown in Figure 6, which plots two orthogonal cross sections through the disc. The disc remains thin, but exhibits a substantial warp with a structure dominated by the zero-frequency tilt mode and the three longest wavelength normal modes of the disc $j = 1, 2, 3$. We conclude that vector resonant relaxation can excite a coherent warp in an initially thin, flat disc.

In two-body relaxation the perturbing forces from a surrounding cluster of stars usually thicken a disc, rather than warping it. For example, the observed thickness of the Galactic disc in the solar neighborhood has been used to constrain the effective mass of the objects comprising the Galaxy’s dark-matter halo (e.g., Lacey & Ostriker 1985). Warping, rather than thickening, occurs in this case for two main reasons:

(i) Vector resonant relaxation arises through the torque from a stellar orbit after averaging over mean anomaly and argument of pericentre, and this averaged torque has much less small-scale power than the forces exerted in the passage of a nearby star (cf. Fig. 5). More quantitatively, consider

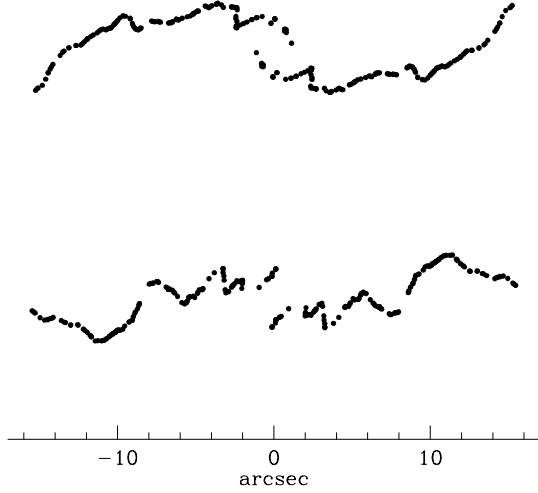


Figure 7. Identical to Figure 6, except that the gravitational interactions among the disc stars have been turned off. The disc-star inclinations are much more irregular at small radii.

two nearby stars on circular orbits with semi-major axes a and $a + \Delta a$, and relative inclination $I \lesssim \Delta a/a$; torques from stars at larger relative inclinations are smaller and can be neglected for this argument. The time-averaged or secular torque between the two orbits is $T \sim Gm^2/\Delta a$. For a radial density profile $n \sim n_0 r^{-\gamma}$, the number of stars in this semi-major axis and inclination range is $\Delta N \sim n_0 a^{2-\gamma} I^2 \Delta a \sim n_0 a^{-\gamma} (\Delta a)^3$. The total stochastic torque generated by these stars is then $(\Delta N)^{1/2} T \propto n_0^{1/2} Gm^2 (\Delta a)^{1/2}$. This is an increasing function of Δa , showing that the secular torque on the disc is dominated by large-scale fluctuations. A nonzero eccentricity for either the cluster or disk stars further reduces the small-scale power.

(ii) As suggested by equations (58), the excitation of normal modes in the disc is reduced if the coherence time of the torque exceeds the inverse frequency of the normal mode, and the coherence time for vector resonant relaxation is longer than the inverse frequencies associated with small-scale normal modes in the disc. To illustrate the importance of this effect, Figure 7 shows the results of a simulation identical to that leading to Figure 6, except that the masses of the disc stars have been reduced to nearly zero. Reducing the disc-star masses decreases all oscillation frequencies Λ_i , since these are proportional to mass in Laplace–Lagrange theory. In the limit of near-zero mass, the interaction between the disc stars becomes negligible as described in Sec. 4.1.1 and $\langle Q_i Q_j \rangle$ becomes independent of Λ_i . Figure 7 shows that in this limit the warp becomes much more irregular and less spatially coherent, because both large-scale and small-scale modes are excited.

Figure 8 shows the normal mode power and cross-correlation as a function of the average wavelength, $\lambda_i = 2(r_{\max} - r_{\min})/i$. The y -axis shows $\langle Q_{i+k} Q_{i-k} \rangle$ for $k = 0, 1, \text{ and } 2$, where Q_i is the amplitude of the i^{th} normal mode (see Fig. 4). The circles show the mean of Q_i^2 and the shaded

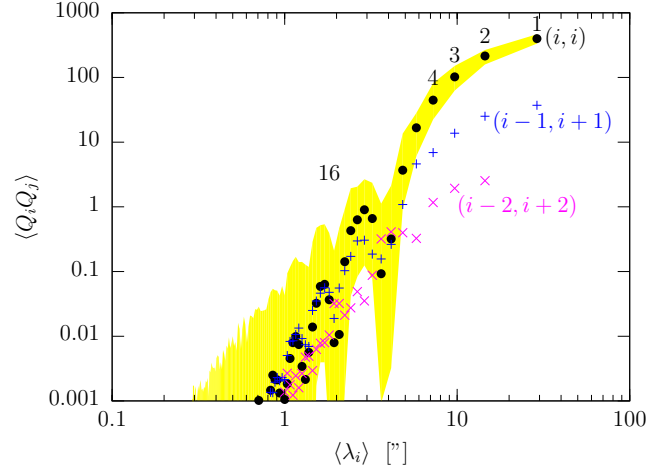


Figure 8. The typical amplitudes of normal modes (arbitrary scale), as a function of their average wavelength. The circles mark the mean of the squared amplitudes of normal modes for a random realization of the disc for each i , and the 95% confidence interval is shaded. Plusses and crosses show the cross-correlation between various normal modes for comparison. In this case, the distribution is symmetric around 0, and the symbols are placed at the boundary of the 95% confidence interval. The modes $i = 1, 2, 3, 4$, and 16 shown in Fig. 4 are labelled. The torques are assumed to be constant during the 6 Myr lifetime of the disc with an amplitude corresponding to the RMS torque (eq. 80). The high-frequency, short-wavelength normal modes are suppressed.

region shows the 95% confidence interval for a random realization of the disc. In contrast, the cross correlation of normal modes has zero mean, for these elements the symbols correspond to the upper boundary of the 95% interval. The calculations are based on equations (68) and (80). The long-wavelength modes dominate the disc, and modes with wavelength $\lesssim 1$ arcsec are suppressed by some five orders of magnitude. Note that the predicted amplitude of the longest wavelength modes ($i \leq 6$) exhibits only a small scatter between various realizations of the disc. Although the different normal modes are not independent, the cross correlation between modes with increasingly different average wavelengths are clearly more and more suppressed. The RMS warping of the disc then follows from eq. (63). Figure 8 shows that a coherent torque tilts and warps the disc in a way that its shape is reminiscent of only a few long wavelength modes.

6 DISCUSSION

The massive young stars observed in the Galactic centre at radii $\sim 0.05\text{--}0.5$ pc from the central black hole may have formed in a thin, flat disc. Using the best available estimates for the mass, age, and other properties of the disc and the cluster of old stars in which it is embedded, we have shown that the disc naturally and inevitably develops a strong warp through vector resonant relaxation with the cluster. We suggest that this mechanism explains the large ($\sim 60^\circ$) warp that is observed in the disc.

We have modelled the gravitational torques among the disc stars and between the disc stars and the surrounding old cluster. Our models are based on Laplace–Lagrange theory, in which the secular gravitational interactions of

the disc stars are mathematically equivalent to the interactions in a system of masses connected by springs. Laplace–Lagrange theory assumes that the relative inclinations are small, $\Delta_{jk} \equiv |a_j I_j - a_k I_k| / |a_j - a_k| \ll 1$. For the simulation shown in Figure 6, the maximum value of Δ_{jk} was 2.8, indicating that Laplace–Lagrange theory has been extended beyond its domain of applicability but should still be qualitatively correct.

In Laplace–Lagrange theory, the disc dynamics can be decomposed into normal modes. The eigenfrequencies of the normal modes in our models span a vast range of time-scales (cf. Fig. 3). The high-frequency normal modes are an unphysical consequence of the assumption that the disc orbits are precisely circular and that the inclinations are small compared to the separation between stars; in fact the highest frequencies correspond to modes involving only two adjacent stars. However, our results should not be affected by this shortcoming since the high-frequency modes are not excited efficiently by torques from the cluster stars (cf. Fig. 8).

The frequencies depend monotonically on the wavelength of the mode: oscillation times π/Λ of about 13 Myr correspond to wavelengths of ~ 0.4 pc (10 arcsec) (cf. blue curve in Fig. 4); faster or slower modes have smaller and longer wavelengths, respectively. The frequencies and the shapes of the slow normal modes are insensitive to the details of the stellar mass function so long as the large-scale surface density of the disc is fixed.

The growth of a given mode saturates after about a half oscillation period. The low-frequency, long-wavelength modes are excited to much larger amplitudes than high-frequency, short-wavelength modes, both because the secular torques couple more strongly to long-wavelength modes, and because the low-frequency modes saturate after a longer time (an equivalent statement is that the amplitudes of the high-frequency modes are adiabatic invariants).

The most important free parameter in our models is the effective mass $m_2 = \langle m^2 \rangle / \langle m \rangle$ of the stars and other irregularities (e.g., clusters, gas clouds, etc.) in the cluster; the simulation in Figure 6 assumes $m_2 = 10 M_\odot$, which is likely to be an underestimate. A larger value of m_2 increases the warp amplitude proportional to $m_2^{1/2}$.

For simplicity our simulations are done using time-independent torques from a cluster. For a spherical cluster, this approximation is valid if the disc age is less than the vector resonant relaxation time, since this is approximately the same as the coherence time. A rough measure of the validity of this approximation is given by Figure 7, which shows the evolution of the orientations of the stars in a disc of zero mass: since the disc self-gravity has been turned off in this figure, the stars behave in the same manner as random stars in the spherical cluster, so the approximation that the perturbing forces from the cluster are constant is valid if the inclinations of the stars in this Figure are small. Evidently the approximation of constant forces is good for the outer parts of the cluster, where the relaxation time is relatively long, and suspect in the inner parts.

Both of our major approximations – Laplace–Lagrange theory and constant perturbing forces – are more accurate if the effective mass is smaller than the assumed value $m_2 = 10 M_\odot$ and worse if it is larger.

We also assumed that the cluster is spherical on av-

erage (i.e., apart from Poisson fluctuations due to individual stars), that the orientations of cluster star orbits are uncorrelated, that there is no back-reaction from the disc on the cluster, that the cluster stars are on circular orbits, and that the cluster mass profile $M(r)$ (eq. 8) can be determined from the luminosity distribution $L(r)$ assuming constant mass-to-light ratio. Under these approximations, the fractional deviation from sphericity at radius $r \gtrsim 0.2$ pc is roughly $\sqrt{m_2/M(r)} = 0.009 \sqrt{m_2/10 M_\odot} (r/0.1 \text{ pc})^{-0.63}$. The deviation from sphericity may be larger if the cluster is flattened due to rotation; however, Trippe et al. (2008) estimate the rotation speed of the cluster to be $v_{\text{rot}}(r) = (3.6 \pm 0.8) \text{ km s}^{-1} (r/0.1 \text{ pc})$ within 1 pc. The rotational flattening of the cluster is then roughly $v_{\text{rot}}^2/\sigma^2 \sim 2 \times 10^{-4} (r/0.1 \text{ pc})^3$, smaller than the stochastic flattening for $r \lesssim 0.3$ pc. The flattening of the overall mass distribution due to the disc is comparable to the stochastic flattening (see discussion following eq. 26) so the neglect of this contribution probably does not seriously invalidate our results. The justification for neglecting the back-reaction of the disc is described at the end of §4.2. The assumption that the orientations of cluster star orbits are uncorrelated is harder to justify, and to do so will require a self-consistent simulation of both the disc and cluster stars (see the discussion at the end of this section). The assumption that the stars in the cluster are on circular orbits is unrealistic – the scalar resonant relaxation time is much less than the age of the Galaxy so we expect the eccentricity distribution to be $dn \propto e de$. This defect will be removed in future calculations.

Bregman & Alexander (2009) have suggested that warps in accretion discs surrounding black holes in the centres of galaxies – in particular, the $\sim 10^\circ$ warp in the maser disc in NGC 4258 – may arise from resonant relaxation with the surrounding stellar cluster. In accretion discs the warp dynamics may also be affected by gas pressure, viscous dissipation, and radial transport of mass and angular momentum (Pringle 1992; Lodato & Pringle 2007), as well as opacity and radiation pressure in radiatively efficient discs (Petterson 1977; Maloney, Begelman, & Pringle 1996).

The treatment in the present paper does not address several important issues:

- What are the characteristics of the disc after vector resonant relaxation excites a large warp – in particular, large enough that the Laplace–Lagrange treatment is invalid?
- Can vector resonant relaxation create structures that resemble the second, ‘counter-clockwise’ disc seen at the Galactic centre? A mechanism to form both the clockwise and counter-clockwise discs from a single thin, flat precursor would explain why stars in both discs have the same age.
- The WR/O stars in the disc(s) are much more massive than the old cluster stars. What is the analog of dynamical friction for vector resonant relaxation and what role does it play in determining the disc structure?

These questions can be addressed most effectively by ‘N-ring’ simulations that follow the evolution of a set of N axisymmetric rings, each representing the smeared-out mass density in a Keplerian orbit after averaging over mean anomaly and argument of pericentre. Each ring exerts a torque on every other ring, and the simulation follows the precession of the rings in response to these torques. We have written a code to carry out these simulations and are cur-

rently using it to follow the evolution of stellar systems that resemble the central parsec of the Galaxy.

We thank Yuri Levin for useful discussions and the anonymous referee for suggestions that substantially improved the paper. This research was supported in part by NASA grant NNX08AH24G and NSF grant AST-0807432. B.K. acknowledges support by NASA through Einstein Postdoctoral Fellowship grant number PF9-00063 awarded by the Chandra X-ray Center, which is operated by the Smithsonian Astrophysical Observatory for NASA under contract NAS8-03060, and partial support by OTKA grant 68228.

APPENDIX A: THE MICROCANONICAL ENSEMBLE IN LAPLACE–LAGRANGE THEORY

We have argued in §2 that vector resonant relaxation among the stars of the Galactic-centre disc(s) is unimportant. However, there is a wide range of disc ages and environments for which internal vector resonant relaxation may be the dominant process of dynamical relaxation. A particularly simple case is an isolated disc with age much larger than the vector resonant relaxation time. Isolated discs conserve total energy and angular momentum; moreover, if vector resonant relaxation is the only important dynamical process the semi-major axis and eccentricity of each star is conserved. According to the usual principles of statistical mechanics, the probability distribution of such discs (the microcanonical ensemble) should be uniform in the manifold of phase space that is determined by these conserved quantities.

For sufficiently small inclinations, the Hamiltonian of the disc is given by the Laplace–Lagrange form (32). Since this Hamiltonian is quadratic in the coordinates and momenta, the equations of motion are linear and therefore integrable. Thus in principle an isolated disc with sufficiently small eccentricities and inclinations exhibits no resonant relaxation. Our assumption is that higher-order terms that we have neglected in the Hamiltonian lead to relaxation to an equilibrium state that can be approximately described using the statistical mechanics of the quadratic Hamiltonian – just as occasional collisions in an ideal gas lead to a thermal equilibrium that can be described using the quadratic Hamiltonian $H = \frac{1}{2}p^2/m$.

The Hamiltonian H and the angular-momentum deficit Z (eq. 50) are both conserved. An important combination of these is

$$\Gamma(\mathbf{q}, \mathbf{p}) \equiv \frac{H(\mathbf{q}, \mathbf{p})}{Z(\mathbf{q}, \mathbf{p})} = \frac{\mathbf{p}^T \mathbf{A} \mathbf{p} + \mathbf{q}^T \mathbf{A} \mathbf{q}}{\mathbf{p}^T \mathbf{p} + \mathbf{q}^T \mathbf{q}}. \quad (\text{A1})$$

Since Γ has units of inverse time we call it the frequency parameter of the disc¹².

We can re-write the last of these expressions as

$$\Gamma(\mathbf{P}, \mathbf{Q}) = \frac{\sum_{i=0}^{N-1} \Lambda_i (P_i^2 + Q_i^2)}{\sum_{i=0}^{N-1} (P_i^2 + Q_i^2)}, \quad (\text{A2})$$

which shows that Γ can only span a limited range of values, from Λ_{\min} to Λ_{\max} where these are the minimum and maximum eigenvalues of \mathbf{A} .

We may also assume that the conserved x and y components of the angular momentum L_x, L_y are both zero, since this can be ensured by choosing the z -axis of the coordinate system to be parallel to the total angular-momentum vector. Then from equation (49) $P_0 = Q_0 = 0$.

To analyse the properties of the microcanonical ensemble, we first find the density of states $\omega_N(E, C)$, defined so that $\omega_N(E, C)dEdC$ is the volume in $2(N-1)$ -dimensional phase space in which the energy and angular-momentum deficit are in the ranges $(E, E + dE)$ and $(C, C + dC)$. Thus¹³

$$\begin{aligned} \omega_N(E, C) &= \int \prod_{i=1}^{N-1} dP_i dQ_i \delta[E - H(\mathbf{P}, \mathbf{Q})] \delta[C - Z(\mathbf{P}, \mathbf{Q})] \\ &= \int \prod_{i=1}^{N-1} dP_i dQ_i \delta(E - \mathbf{P}^T \mathbf{A} \mathbf{P} + \mathbf{Q}^T \mathbf{A} \mathbf{Q}) \delta(C - \mathbf{P}^T \mathbf{P} - \mathbf{Q}^T \mathbf{Q}). \end{aligned} \quad (\text{A3})$$

We use the identity

$$\delta(x) = \frac{1}{2\pi i} \int_{-i\infty}^{i\infty} dt e^{tx}. \quad (\text{A4})$$

Then

$$\begin{aligned} \omega_N(E, C) &= -\frac{1}{4\pi^2} \int \prod_{i=1}^{N-1} dP_i dQ_i \int_{-i\infty}^{i\infty} dt \int_{-i\infty}^{i\infty} dt' \exp[tE + t'C - t(\mathbf{P}^T \mathbf{A} \mathbf{P} + \mathbf{Q}^T \mathbf{A} \mathbf{Q}) - t'(\mathbf{P}^T \mathbf{P} + \mathbf{Q}^T \mathbf{Q})] \\ &= -\frac{1}{4\pi^2} \int \prod_{i=1}^{N-1} dP_i dQ_i \int_{-i\infty}^{i\infty} dt e^{tE} \int_{-i\infty}^{i\infty} dt' e^{t'C} \exp\left[-\sum_{i=1}^{N-1} (P_i^2 + Q_i^2)(t\Lambda_i + t')\right]. \end{aligned} \quad (\text{A5})$$

The next step is to exchange the order of integration, but this cannot be done immediately as $\int dP dQ \exp[-(P^2 + Q^2)(t\Lambda + t')]$ is not absolutely convergent for imaginary t and t' . However, using the identity $1 = \exp(uC) \exp[-u \sum_{i=1}^{N-1} (P_i^2 + Q_i^2)]$ (recall $P_0 = Q_0 = 0$) we can rewrite the double integral as

$$\omega_N(E, C) = -\frac{e^{uC}}{4\pi^2} \int \prod_{i=1}^{N-1} dP_i dQ_i \int_{-i\infty}^{i\infty} dt e^{tE} \int_{-i\infty}^{i\infty} dt' e^{t'C} \exp\left[-\sum_{i=1}^{N-1} (P_i^2 + Q_i^2)(t\Lambda_i + t' + u)\right], \quad (\text{A6})$$

¹² Note that Γ used here is not related to $\Gamma_{nm}(t)$ denoting the correlation function in the main text.

¹³ The system we are studying resembles the celebrated spherical model for a ferromagnet (Berlin & Kac 1952) and much of our analysis is borrowed from the literature on that problem.

and the integral over $dP_i dQ_i$ is now absolutely convergent for $u > 0$. The order of integration can now be exchanged so that the $2(N-1)$ -dimensional integral over phase space can be done:

$$\omega_N(E, C) = -\frac{\pi^{N-3}}{4} \int_{-i\infty}^{i\infty} dt e^{tE} \int_{u-i\infty}^{u+i\infty} ds e^{sC} \prod_{i=1}^{N-1} (s + t\Lambda_i)^{-1} = -\frac{\pi^{N-3}}{4} \int_{-i\infty}^{i\infty} dt \int_{u-i\infty}^{u+i\infty} ds \exp \left[tE + sC - \sum_{i=1}^{N-1} \log(s + t\Lambda_i) \right], \quad (\text{A7})$$

where $s \equiv u + t'$.

For $N \gg 1$ we can evaluate this integral by the method of stationary phase. Denoting the quantity in square brackets as $g(s, t)$, the dominant contribution to the integral comes from near the points (s_0, t_0) at which $\partial g / \partial s = \partial g / \partial t = 0$, that is,

$$C = \sum_{i=1}^{N-1} \frac{1}{s_0 + t_0 \Lambda_i}, \quad E = \sum_{i=1}^{N-1} \frac{\Lambda_i}{s_0 + t_0 \Lambda_i}. \quad (\text{A8})$$

We now show that s_0 and t_0 are real. Since E , C , u , and Λ_i are real, the imaginary part of these equations reads

$$w_0 \Im(s_0) + w_1 \Im(t_0) = 0, \quad w_1 \Im(s_0) + w_2 \Im(t_0) = 0, \quad (\text{A9})$$

where

$$w_n \equiv \sum_{i=1}^{N-1} \frac{\Lambda_i^n}{D(\Lambda_i, s_0, t_0)}, \quad D(\Lambda_i, s_0, t_0) = [\Re(s_0) + \Re(t_0)\Lambda_i]^2 + [\Im(s_0) + \Im(t_0)\Lambda_i]^2. \quad (\text{A10})$$

Thus either $\Im(s_0) = \Im(t_0) = 0$ or

$$w_0 w_2 - w_1^2 = \frac{1}{2} \sum_{i=1}^{N-1} \sum_{j=1}^{N-1} \frac{(\Lambda_i - \Lambda_j)^2}{D(\Lambda_i, s_0, t_0) D(\Lambda_j, s_0, t_0)} \quad (\text{A11})$$

must vanish. This condition is only satisfied in the trivial case when all of the eigenvalues Λ_i are equal. Thus s_0 and t_0 must be real.

Let the real numbers s_c and t_c denote the locations where the integration contours cross the real axis in the complex s and t planes. In equation (A7) $s_c = u$ and $t_c = 0$. In the method of stationary phase the contours are deformed to cross the real axes at $s_c = s_0$ and $t_c = t_0$. During this deformation s_c and t_c cannot cross the poles at $s + t\Lambda_i = 0$. Each such pole defines a line in the (s_c, t_c) plane and in its journey from $(u, 0)$ to (s_0, t_0) the point (s_c, t_c) cannot cross any of these lines. This constraint implies that

$$t > -\frac{s}{\Lambda_{\min}} \quad \text{if } s < 0; \quad t > -\frac{s}{\Lambda_{\max}} \quad \text{if } s \geq 0 \quad (\text{A12})$$

where Λ_{\min} is the smallest eigenvalue (other than $\Lambda_0 = 0$) and Λ_{\max} is the largest, i.e., $0 = \Lambda_0 < \Lambda_{\min} \leq \Lambda_i$, $i = 1, \dots, N \leq \Lambda_{\max}$.

To evaluate the integral (A7) we expand the argument $g(s, t)$ of the exponential in a Taylor series around (s_0, t_0) . We have

$$\frac{\partial^2 g}{\partial s^2}(s_0, t_0) = w_0, \quad \frac{\partial^2 g}{\partial s \partial t}(s_0, t_0) = w_1, \quad \frac{\partial^2 g}{\partial t^2}(s_0, t_0) = w_2, \quad \text{where } w_n = \sum_{i=1}^{N-1} \frac{\Lambda_i^n}{(s_0 + t_0 \Lambda_i)^2}, \quad (\text{A13})$$

which is consistent with (A10) since s_0 and t_0 are now known to be real. Then

$$\omega_N(E, C) \simeq -\frac{\pi^{N-3}}{4} \int_{-i\infty}^{i\infty} dt \int_{u-i\infty}^{u+i\infty} ds \exp \left[g(s_0, t_0) + \frac{1}{2} w_0 (s - s_0)^2 + w_1 (s - s_0)(t - t_0) + \frac{1}{2} w_2 (t - t_0)^2 \right]. \quad (\text{A14})$$

We introduce new integration variables (v, v') by $s = s_0 + iv$, $t = t_0 + i(v' - v w_1 / w_2)$ and the integral becomes

$$\begin{aligned} \omega_N(E, C) &\simeq \frac{\pi^{N-3}}{4} \frac{\exp[g(s_0, t_0)]}{\int_{-\infty+i(s_0-u)}^{\infty+i(s_0-u)} dv \exp \left(-\frac{w_0 w_2 - w_1^2}{2w_2} v^2 \right)} \int_{i[t_0+(s_0-u)w_1/w_2]-\infty}^{i[t_0+(s_0-u)w_1/w_2]+\infty} dv' \exp \left[-\frac{1}{2} w_2 (v')^2 \right] \\ &= \frac{\pi^{N-2}}{2\sqrt{w_0 w_2 - w_1^2}} \exp \left[t_0 E + s_0 C - \sum_{i=1}^{N-1} \log(s_0 + t_0 \Lambda_i) \right]; \end{aligned} \quad (\text{A15})$$

the argument of the square root is positive, as seen from equation (A11).

The entropy of the microcanonical ensemble is

$$S(N, E, C) = \log \omega_N(E, C) = \left[t_0 E + s_0 C - \sum_{i=1}^{N-1} \log(s_0 + t_0 \Lambda_i) \right] - \frac{1}{2} \log(w_0 w_2 - w_1^2) + \text{const}, \quad (\text{A16})$$

where Boltzmann's constant has been set to unity. For fixed values of s_0 , t_0 , Λ_i the content of the square bracket grows linearly with N while the second term grows only logarithmically. Thus as $N \rightarrow \infty$ we may drop the second term, and

$$S(N, E, C) = t_0 E + s_0 C - \sum_{i=1}^{N-1} \log(s_0 + t_0 \Lambda_i) + \text{const}. \quad (\text{A17})$$

The temperature T is defined by

$$\frac{1}{T} = \left(\frac{\partial S}{\partial E} \right)_C = t_0 + \left(E \frac{\partial t_0}{\partial E} + C \frac{\partial s_0}{\partial E} \right)_C - \sum_{i=1}^{N-1} \frac{1}{s_0 + t_0 \Lambda_i} \left(\frac{\partial s_0}{\partial E} + \Lambda_i \frac{\partial t_0}{\partial E} \right)_C. \quad (\text{A18})$$

Using equations (A8), this and the analogous expression for $\partial S/\partial C$ simplify to

$$\frac{1}{T} = \left(\frac{\partial S}{\partial E} \right)_C = t_0, \quad \left(\frac{\partial S}{\partial C} \right)_E = s_0. \quad (\text{A19})$$

We now investigate whether the solution to equations (A8) exists and is unique. By manipulating the identity $N - 1 = \sum_{i=1}^{N-1} (s_0 + t_0 \Lambda_i)/(s_0 + t_0 \Lambda_i)$ it is easy to see that

$$s_0 C + t_0 E = N - 1. \quad (\text{A20})$$

With this result, equations (A8) can be combined to give

$$\Gamma = \frac{E}{C} = h(N, C, \Gamma; t_0) \quad \text{where} \quad h(N, C, \Gamma; t) \equiv \frac{\sum_{i=1}^{N-1} \Lambda_i [N - 1 + tC(\Lambda_i - \Gamma)]^{-1}}{\sum_{i=1}^{N-1} [N - 1 + tC(\Lambda_i - \Gamma)]^{-1}}. \quad (\text{A21})$$

This non-linear equation can be solved for t_0 given E , C , and N . Furthermore we have

$$\frac{\partial h}{\partial t}(N, C, \Gamma; t) = - \frac{C(N-1)}{2 \left[\sum_{i=1}^{N-1} [N - 1 + tC(\Lambda_i - \Gamma)]^{-1} \right]^2} \sum_{i,j=1}^{N-1} \frac{(\Lambda_i - \Lambda_j)^2}{[N - 1 + tC(\Lambda_i - \Gamma)]^2 [N - 1 + tC(\Lambda_j - \Gamma)]^2}, \quad (\text{A22})$$

which is negative-definite, so h decreases monotonically with t . Thus there is at most one solution for t_0 for given E , C , and N . Using equation (A20) to eliminate s_0 from the constraints (A12), and recalling that $\Lambda_{\min} \leq \Gamma \leq \Lambda_{\max}$ (see the discussion following eq. A2) we find that t_0 is restricted to the range

$$t_{\min} \equiv - \frac{N-1}{C(\Lambda_{\max} - \Gamma)} < t_0 < t_{\max} \equiv \frac{N-1}{C(\Gamma - \Lambda_{\min})}. \quad (\text{A23})$$

Note that $t_{\min} < 0$ and $t_{\max} > 0$, and

$$h(t_{\min}) = \Lambda_{\max}, \quad h(t_{\max}) = \Lambda_{\min}. \quad (\text{A24})$$

Thus $h(t)$ decreases monotonically from Λ_{\max} to Λ_{\min} as t grows over its allowed range from t_{\min} to t_{\max} . Since Γ must lie between Λ_{\max} to Λ_{\min} for any initial condition, equation (A21) always has a unique solution for t_0 given E , C , and N , and equation (A20) then gives a unique solution for s_0 .

Note that $h(N, C, \Gamma; 0) = \sum_{i=1}^{N-1} \Lambda_i / N \equiv \Lambda_A$, the arithmetic mean of the eigenvalues. Thus if $\Gamma > \Lambda_A$, $t_0 < 0$ (negative temperature) while if $\Gamma < \Lambda_A$ then $t_0 > 0$ (positive temperature).

The one-particle distribution function $f_1(P_1, Q_1)$ is defined so that $f(P_1, Q_1) dP_1 dQ_1$ is the probability that P_1, Q_1 lie in the phase-space volume element $dP_1 dQ_1$. We have

$$\begin{aligned} f_1(P_1, Q_1) &= \frac{1}{\omega_N(E, C)} \int \prod_{i=2}^{N-1} dP_i dQ_i \delta \left[E - \Lambda_1 (P_1^2 + Q_1^2) - \sum_{i=2}^{N-1} \Lambda_i (P_i^2 + Q_i^2) \right] \delta \left[C - P_1^2 - Q_1^2 - \sum_{i=2}^{N-1} (P_i^2 + Q_i^2) \right] \\ &= \frac{\omega_{N-1} \left[E - \Lambda_1 (P_1^2 + Q_1^2), C - P_1^2 - Q_1^2 \right]}{\omega_N(E, C)}. \end{aligned} \quad (\text{A25})$$

Since $N \gg 1$ the differences between the numerator and denominator in the solutions of equations (A8) for s_0 and t_0 are negligible, as are the differences in w_k defined by equation (A13). With this approximation and the use of equation (A15) we have

$$f_1(P_1, Q_1) = \frac{s_0 + t_0 \Lambda_1}{\pi} \exp \left[- (s_0 + t_0 \Lambda_1) (P_1^2 + Q_1^2) \right]. \quad (\text{A26})$$

Similar arguments show that the two-particle distribution function is the product of one-particle functions, $f_2(P_1, Q_1, P_2, Q_2) = f(P_1, Q_1) f(P_2, Q_2)$, etc.

The average energy in a single normal mode is

$$E_i \equiv \Lambda_i \langle P_i^2 + Q_i^2 \rangle = \frac{\Lambda_i}{s_0 + t_0 \Lambda_i}, \quad (\text{A27})$$

where the last equality follows from (A26). If $s_0 = 0$ each mode contains the same energy; in other words, there is equipartition of energy or the power spectrum is independent of the frequency Λ_i . We shall call this ‘white noise’ – a small abuse of language since in most applications white noise corresponds to constant energy per unit frequency rather than per mode. If $s_0 < 0$ then E_i grows as the frequency Λ_i decreases (red noise). If $s_0 > 0$ the energy per mode grows as the frequency grows (blue noise). The condition $s_0 = 0$ corresponds to $\Gamma = N / \sum_{i=1}^{N-1} \Lambda_i^{-1} \equiv \Lambda_H$, the harmonic mean of the eigenvalues. Since $\Lambda_H < \Lambda_A$ (harmonic mean is less than the arithmetic mean), we have three cases,

- (i) Positive temperature, red noise:

$$\Lambda_{\min} < \Gamma < \Lambda_H, \quad -\frac{(N-1)\Lambda_{\min}}{C(\Gamma - \Lambda_{\min})} < s_0 < 0, \quad \frac{(N-1)}{C(\Gamma - \Lambda_{\min})} > t_0 > \frac{N-1}{C\Lambda_H};$$

(ii) Positive temperature, blue noise:

$$\Lambda_H < \Gamma < \Lambda_A, \quad 0 < s_0 < \frac{N-1}{C}, \quad \frac{N-1}{C\Lambda_H} > t_0 > 0;$$

(iii) Negative temperature, blue noise:

$$\Lambda_A < \Gamma < \Lambda_{\max}, \quad \frac{N-1}{C} < s_0 < \frac{(N-1)\Lambda_{\max}}{C(\Lambda_{\max} - \Gamma)}, \quad 0 > t_0 > -\frac{(N-1)}{C(\Lambda_{\max} - \Gamma)}. \quad (\text{A28})$$

Microcanonical ensembles characterized by red noise tend to exhibit warps, because there is more power in low-frequency, long-wavelength modes.

A1 Simulations of the microcanonical ensemble

We want to generate realizations of a relaxed disc containing N stars on circular orbits, with masses and semi-major axes m_i , a_i , $i = 0, \dots, N-1$. The disc is specified initially by its energy E and angular-momentum deficit C . The procedure is: (i) compute the matrices \mathbf{A} (eq. 40) and \mathbf{O} (eq. 42) and the eigenvalues Λ_i of \mathbf{A} . (ii) Set $\Gamma = E/C$; if Γ lies outside the interval $[\Lambda_{\min}, \Lambda_{\max}]$ spanned by the non-zero eigenvalues Λ_i , $i = 1, N-1$ then these values of E and C cannot be achieved by a disc with the given masses and semi-major axes. Otherwise, find the unique solution t_0 to the non-linear equation (A21) and then find s_0 from the linear equation (A20). (iii) Set $P_0 = Q_0 = 0$. Choose (P_i, Q_i) , $i = 1, \dots, N-1$ at random from the Gaussian distribution (A26). (iv) Set $p_i = \sum_{j=1}^{N-1} O_{ij} P_j$, $q_i = \sum_{j=1}^{N-1} O_{ij} Q_j$, then find the inclinations I_i and nodes Ω_i of the N stars using equations (36). The resulting disc will have energy E and angular-momentum deficit C that are within $O(N^{-1/2})$ of the assumed initial conditions (although the differences can still be substantial if the energy or angular-momentum deficit is dominated by a small number of modes).

Note that discs with different values of E and C but the same value of $\Gamma = E/C$ have $t_0 \propto 1/C$ (by eq. A21) and $s_0 \propto 1/C$ (by eq. A20) so the distributions of P_i , Q_i , p_i , q_i , and I_i scale as \sqrt{C} (by eq. A26). Thus, apart from this trivial scaling, the relaxed discs with a given distribution of stellar masses and semi-major axes form a one-parameter family defined by the frequency parameter Γ .

We generate microcanonical ensembles of discs having the same distribution of stellar masses and semi-major axes as in the simulations described at the start of §5. The eigenvalues Λ_i in this disc span a range of 10^7 in magnitude (Fig. 3). The largest eigenvalues arise because the interactions of stars that happen to have similar semi-major axes, $\Delta a/a \ll 1$, are unrealistically strong, essentially because the approximation that the Hamiltonian is quadratic is only valid so long as the inclinations satisfy $I \ll \Delta a/a$. Thus the calculations presented here may not accurately represent the thickness of the equilibrium disc.

A sample simulation with frequency parameter $\Gamma = (10^5 \text{ yr})^{-1}$ is shown in Figure A1. The two plots show $I \cos \Omega$ and $I \sin \Omega$ as a function of semi-major axis; the visible high-mass stars ($m > 20 M_\odot$) are marked with solid blue circles, and the low-mass stars are marked by open red circles. The vertical axis is arbitrary since the disc properties can be scaled to other energies, as described above.

As discussed above, the high-frequency modes are unphysical, because the interactions between adjacent stars are unrealistically strong. However, most of the structure visible in Figure A1 arises from low-frequency modes, which are largely independent of the strong interactions between close neighbors. To illustrate this, we have experimented with softening the interaction potential according to equation (37). We find that softenings as large as $\epsilon = 0.003$ have very little effect on the appearance of realizations of the disc.

One of the striking features of the disc shown in Figure A1 is the overall warp. To characterize the warp amplitude quantitatively, we first define the inclination vectors $\mathbf{I}_i \equiv I_i(\cos \Omega_i, \sin \Omega_i)$ where I_i and Ω_i are the inclination and node of star i . Then we define the mean and dispersion of the $N_{\mathcal{A}}$ inclination vectors in some semi-major axis range \mathcal{A} by

$$\bar{\mathbf{I}}_{\mathcal{A}} \equiv \frac{1}{N_{\mathcal{A}}} \sum_{i \in \mathcal{A}} \mathbf{I}_i, \quad \sigma_{\mathcal{A}}^2 \equiv \frac{1}{2(N_{\mathcal{A}} - 1)} \sum_{i \in \mathcal{A}} (\mathbf{I}_i - \bar{\mathbf{I}}_{\mathcal{A}})^2; \quad (\text{A29})$$

the factor of two in the second equation arises because $\sigma_{\mathcal{A}}^2$ is the dispersion in one of the two components of the vector \mathbf{I} . In the small-angle approximation within which we are working, the angle between the mean orbit normals in regions \mathcal{A} and \mathcal{A}' is

$$\theta \equiv |\bar{\mathbf{I}}_{\mathcal{A}} - \bar{\mathbf{I}}_{\mathcal{A}'}|. \quad (\text{A30})$$

A measure of the ratio of the warp to the disc thickness is then θ/σ where $\sigma^2 = \frac{1}{2}(\sigma_{\mathcal{A}}^2 + \sigma_{\mathcal{A}'}^2)$. This ratio is independent of the energy E and angular-momentum deficit C so long as the frequency parameter $\Gamma = E/C$ is fixed.

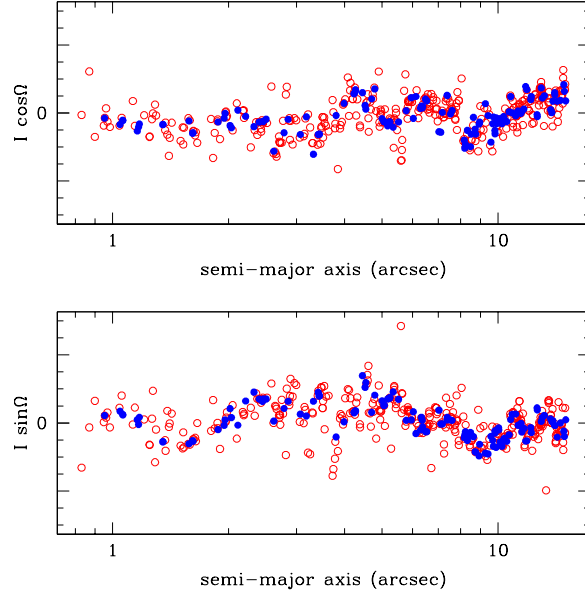


Figure A1. A realization of the microcanonical ensemble. The upper and lower panels show $I \cos \Omega$ and $I \sin \Omega$ for a disc with 500 stars in the mass range 1 to $30 M_{\odot}$; the mass function is given by equation (14) with $\alpha = -0.45$ and the semi-major axis distribution is given by equation (1) with $\gamma = -1.4$. The inner and outer semi-major axes are 1 arcsec and 15.5 arcsec. Solid blue circles denote stars with mass $> 20 M_{\odot}$, corresponding roughly to stars that are visible in current surveys, and open red circles denote stars with smaller masses. The frequency parameter Γ of eq. (A1) equals $(10^5 \text{ yr})^{-1}$.

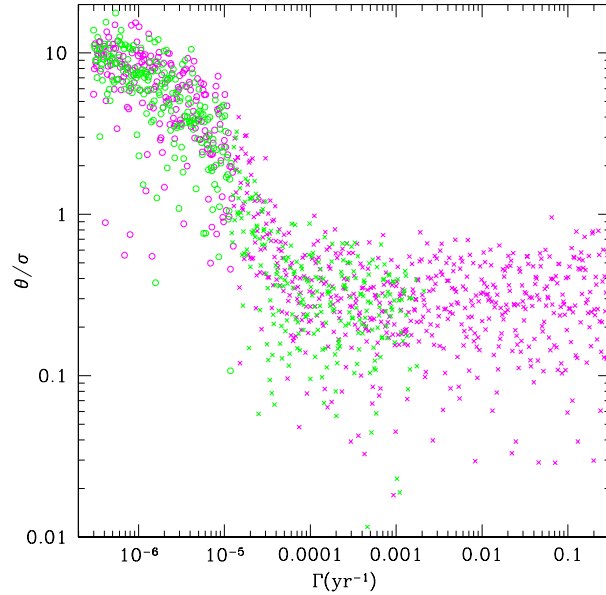


Figure A2. Dimensionless disc warping θ/σ as a function of the frequency parameter Γ . The stellar semi-major axes and masses are chosen by the same procedure used to produce Fig. A1, with a different pseudorandom number seed for each point. The parameter θ is the angle between the mean inclination vectors in the inner and outer third of the disc, and σ is a measure of the thickness of the disc (see text). Magenta and green points correspond to simulations with softening $\epsilon = 0$ and 0.003, respectively. Open circles and crosses represent discs with red and blue noise (Γ less or greater than the harmonic mean of the eigenvalues, Λ_H). Red discs exhibit large warps and blue discs do not.

Warps are associated with large-scale, low-frequency normal modes, and therefore are stronger in microcanonical ensembles dominated by red noise. This is illustrated in Figure A2, which shows the warp ratio θ/σ for the visible stars ($m > 20 M_{\odot}$) in a set of disc realizations with semi-major axes and stellar masses chosen as described at the start of this subsection. Magenta points are from unsoftened simulations and green points are from simulations with softening $\epsilon = 0.003$. The two regions compared, \mathcal{A} and \mathcal{A}' , are the inner and outer third of the disc stars. Discs with red and blue noise ($\Gamma < \Lambda_H$ and $\Gamma > \Lambda_H$, respectively) are marked by open circles and crosses. The warp ratio θ/σ declines from ~ 10 for $\Gamma \ll \Lambda_H$ (substantial warp) to ~ 0.3 for $\Gamma \gg \Lambda_H$ (negligible warp). The softened and unsoftened simulations exhibit the same behavior, except that realizations with $\Gamma \gtrsim 0.003 \text{ yr}^{-1}$ are not present in the softened simulations because the very high-frequency normal modes involving two adjacent stars are suppressed by the softening. We conclude that the microcanonical ensemble can exhibit significant large-scale warps, depending on the initial conditions as described by Γ .

REFERENCES

- Alexander T., 2005, *Phys. Rep.*, 419, 65
 Alexander T., Hopman C., 2009, *ApJ*, 697, 1861
 Bardeen J.M., Petterson J.A., 1975, *ApJ*, 195, L65
 Bartko H., et al., 2009a, *ApJ*, 697, 1741
 Bartko H., et al., 2010, *ApJ*, 708, 834
 Berlin T.H., Kac M., 1952, *Phys. Rev.*, 86, 821
 Binney J., 1992, *ARA&A*, 30, 51
 Binney J., Tremaine S., 2008, *Galactic Dynamics*, 2nd ed. Princeton University Press, Princeton, NJ
 Bregman M., Alexander T., 2009, *ApJ*, 700, L192
 Brodie J.P., Strader J., 2006, *ARA&A*, 44, 193
 Buchholz R.M., Schödel R., Eckart A., 2009, *A&A*, 499, 483
 Christopher M.H., Scoville N.Z., Stolovy S.R., Yun M.S., 2005, *ApJ*, 622, 346
 Cuadra J., Armitage P.J., Alexander R.D., 2008, *MNRAS*, 388, 64
 Dale J.E., Davies M.B., Church R.P., Freitag M., 2009, *MNRAS*, 393, 1016
 Eilon E., Kupi G., Alexander T., 2009, *ApJ*, 698, 641
 Fritz T.K. et al., 2010, arXiv:1003.1717
 Ghez A.M. et al., 2008, *ApJ*, 689, 1044
 Gillessen S., Eisenhauer F., Trippe S., Alexander T., Genzel R., Martins F., Ott, T., 2009, *ApJ*, 692, 1075
 Gürkan M.A., Hopman C., 2007 *MNRAS*, 379, 1083
 Heng K., Tremaine S., 2009, *MNRAS*, in press
 Hobbs A., Nayakshin S., 2009, *MNRAS*, 394, 191
 Hopman C., Alexander T., 2006, *ApJ*, 645, 1152
 Hunter C., Toomre A., 1969, *ApJ*, 155, 747
 Keshet U., Hopman C., Alexander T., 2009, *ApJ*, 698, 64
 Kroupa P., Tout C.A., Gilmore G., 1993, *MNRAS*, 262, 545
 Lacey C.G., Ostriker J.P. 1985, *ApJ*, 299, 633
 Landau L.D., Lifshitz E.M. 2007, *The Classical Theory of Fields*, 4th ed. Butterworth Heinemann, Amsterdam
 Laskar J., 2000, *Phys. Rev. Lett.*, 84, 3240
 Lejeune T., Schaerer D., 2001, *A&A*, 366, 538
 Levin Y., Beloborodov A.M., 2003, *ApJ*, 590, L33
 Löckmann U., Baumgardt H. 2009, *MNRAS*, 394, 1841
 Löckmann U., Baumgardt H., Kroupa P., 2009, *MNRAS*, 398, 429
 Lodato G., Pringle J.E., 2007, *MNRAS*, 381, 1287
 Lu J.R., Ghez A.M., Hornstein S.D., Morris M.R., Becklin E.E., Matthews K., 2009, *ApJ*, 690, 1463
 Maloney P.R., Begelman M.C., Pringle, J.E., 1996, *ApJ*, 472, 582
 Morris M., 1993, *ApJ*, 408, 496
 Murray C.D., Dermott S.F., 1999, *Solar System Dynamics*. Cambridge University Press, Cambridge
 Nayakshin S., 2005, *MNRAS*, 359, 545
 Nayakshin S., Cuadra J., 2005, *A&A*, 437, 437
 Nayakshin S., Dehnen W., Cuadra J., Genzel R., 2006, *MNRAS*, 366, 1410
 Nelson R.W., Tremaine S.D., 1996, in Lahav O., Terlevich E., Terlevich R.J., eds., *Gravitational Dynamics*. Cambridge University Press, Cambridge, p. 73
 O’Leary R.M., Kocsis B., Loeb A., 2009, *MNRAS*, 395, 2127
 Paumard T., et al. 2006, *ApJ*, 643, 1011
 Papaloizou J.C., Terquem C., Lin D.N.C., 1998, *ApJ*, 497, 212
 Perets H.B., Hopman C., Alexander T., 2007, *ApJ*, 656, 709
 Perets H.B., Gualandris A., Kupi G., Merritt D., Alexander T., 2009, *ApJ*, 702, 884
 Pringle J.E., 1992, *MNRAS*, 258, 811

- Pringle J.E., 1996, MNRAS, 281, 357
Petterson J.A., 1977, ApJ, 216, 827
Rauch K.P., Tremaine S., 1996, New Astronomy, 1, 149
Schödel R., et al., 2007, A&A, 469, 125
Schödel R., Merritt D., Eckart A., 2009, A&A, 502, 91
Spitzer, L., Jr. 1958, ApJ, 127, 17
Stewart G.R., Ida S., 2000, Icarus, 143, 28
Subr L., Schovancova J., Kroupa P. 2009, A&A, 496, 695
Tremaine S., 1998, AJ, 116, 2015
Tremaine S., 2005, ApJ, 625, 143
Tremaine S., Weinberg M. D. 1984, MNRAS, 209, 729
Trippe S., et al., 2008, A&A, 492, 419
Ulubay-Siddiki A., Gerhard O., Arnaboldi M., 2009, MNRAS, 398, 535
Yu Q., Tremaine S. 2003, ApJ, 599, 1129
Yu Q., Lu Y., Lin D.N.C., 2007, ApJ, 666, 919